24V-DC/DC Step-down Converter

BACHELOR THESIS
MUCUNGUZI RWAGASORE
ELECTRICAL ENERGY ENGINEERING
AALBORG UNIVERSITY
MARCH 14th 2017

Title:

24V-DC/DC buck converter

Project:

Bachelor Thesis

Project Period:

Jan. 2017 – March. 2017

Student:

Mucunguzi Rwagasore

Supervisors:

Erik Schaltz, AAU

Pages: 40
Appendices: -
Finished 14-03-2017

Abstract:

The project is about a 24V-dc/dc step-down converter. The balance of fuel cell power plant (BOP) components(like pumps, blowers and some electronic controller) needs a 24V supply to be able to operate. Thus, the buck converter is used to supply 24V to BOP. In this project, the buck converter is going to be analysed and designed in Matlab based on the needed requirements. Furthermore, the constant output voltage is needed for good working of the converter. Thus, the converter system will be modelled, therafter the PI type 2 compensator will be analysed and designed. In addition, the Matlab was used to check the stability of the whole system including the compensator. Then, the simulation of the full circuit of converter system with the controller is carried out. The test results is not presented in this project because, more time was spent on designing a buck converter and a suitable controller as the main focus of the project.

Preface

This report has been made during the final semester of the Electrical Energy Engineering BSc. programme at Aalborg University. The purpose with this report is to analyse and design a buck converter to supply a 24V to the Balance of Plant (BOP) components for Fuel cell. In addition, The type 2 compensator will be designed to assure the constant output voltage.

Reading Guide

Most of the individual chapters in the report are introduced and summed up with a section written in the *italic* font. Throughout the report, there will be stated references all listed in the Bibliography. The references are denounced cf. the Harvard Method hence a statement will be referred by [Surname, year]. If more than one reference, these will be separated with a semicolon. If more than one reference from the same year has the same author, these will be denoted with a, b, c, and so forth. This reference refers to the Bibliography where books are referred by author, title, publisher, edition, and year while websites are referred by the author, title, year, and last visit on the website. Figures, Tables, and equations are numbered according to the particular chapter they are placed in. The first Figure in chapter 3 will, therefore, be assigned with Figure number 3.1 and the second 3.2 etc. Descriptive captions for Tables and Figures are found under the Figure or Table in question.

<div align="center">

———————————————

Mucunguzi Rwagasore

</div>

By signing this document, each member of the group confirms that all the group members have participated in the project work, and thereby all members are collectively liable for the contents of the report. Furthermore, all group members confirm that the report does not include plagiarism.

Table of Contents

0.1   Nomenclature

Symbol	Description	Unit
t	Time	$[s]$
T_s	Switching period	$[s]$
f_s	Switching frequency	$[\frac{1}{s}]$
f_m	Pertutbation frequency	$[\frac{1}{s}]$
f_c	Crossover frequency	$[\frac{1}{s}]$
P_x	Specified power	$[W]$
V_x	Specified voltage	$[V]$
I_x	Specified current	$[A]$
R_x	Specified resistance	$[\Omega]$
D	Duty cycle	$[-]$
C	Capacitance	$[F]$
L	Inductance	$[H]$
G_{vc}	Control to output transfer function	$[-]$
G_c	Compensator transfer function	$[-]$
H	Sensor gain	$[-]$

Abbreviations

Symbol	Description
DC	Direct current
D	Duty cycle
CCM	Continuous Conduction Mode
DCM	Discontinuous Conduction Mode
BOP	Balance of plant
CO_2	Carbon dioxide
CH_3OH	Methanol
H_2O	Dihydrogen monoxide(or Water)
O_2	Dioxygen(or Oxygen)
H_2	Hydrogen
PCB	Printed Circuit Board

Introduction 1

The energy demand is continuously increasing today due to different factors like the population growth, the infrastructure development, the increase of the number of vehicles on roads, the industrial development, etc.. The main source of the used energy is fossil fuel which is known to have the serious impacts on the environment like for example the global warming due to its significant emissions of carbon dioxide CO_2 in the atmosphere. The fossil fuel includes coal, natural gas and oil.

In the Figure 1.1, there can be seen the main energy sources in Denmark from year 1990 to 2015, Energistyrelsen [2015].
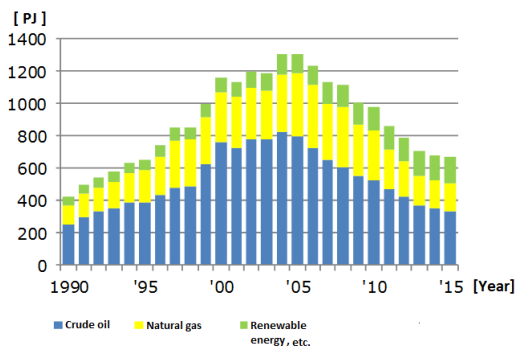

Figure 1.1. The primary energy production in Denmark [Energistyrelsen, 2015].
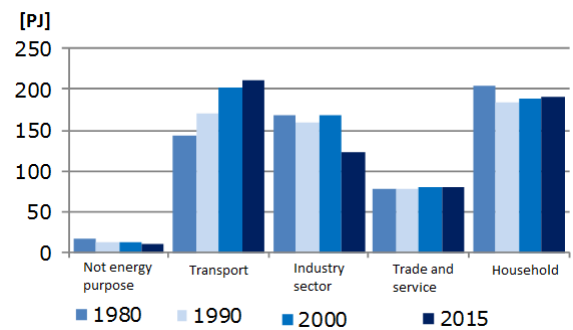

Figure 1.2. The Energy consumption [Energistyrelsen, 2015].

From the Figure 1.1, it can be seen that the oil is most energy production source, and the next is the natural gases, then the renewable and the rest of energy sources. The figure 1.2 shows the energy consumption in different sectors, where the most energy is used in the transport sector, household and in the industries.

The Figure 1.3 shows how the transport energy consumption has grown with different type of transport over the last decade in Denmark.
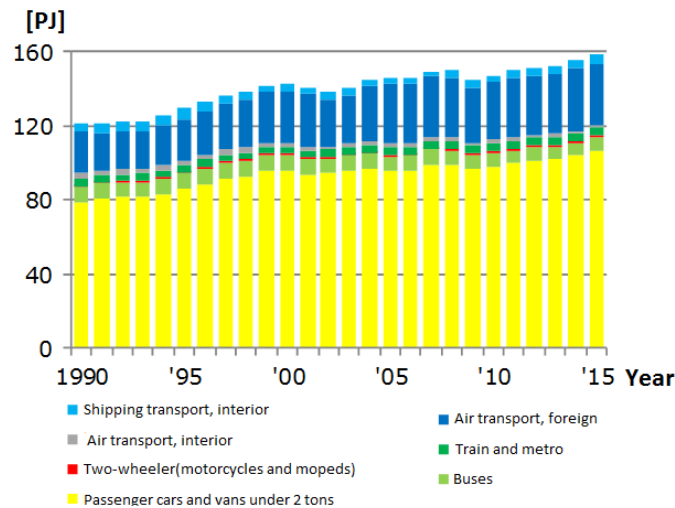
Figure 1.3. The energy consumption in the transport sector [Energistyrelsen, 2015].

As indicated in the Figure 1.3, the energy demand shows a continual growth every year, and the most of this used energy are from fossil fuel like oil, natural gas, etc. as it is indicated in figure 1.1. However, the fossil fuells have a significant impact on people lives and planet in general because of their limit supply, their greenhouse gase emissions when they are burned particularly the carbon dioxide (CO_2) which largely contributes to the global warming and the ecosystem destructions while mining it. Therefore in order to reduce the fossil fuel energy production, there has been put focus on producing the energy from the renewable energy sources, and the Fuel cell is one of the renewable energy source.

1.1 Fuel cell

The Fuel cell normally works like a battery in that it generates the electricity from the electrochemical reaction. The only difference is that the fuel cell produces the electricity continuously as long as the fuel and oxygen are supplied.

For fuel cell devices to generate the electricity, it requires the power system organization as it is shown in Figure 1.4. Under the fuel processing system, there are different components like the fuel reformer, the chemical reactors, the heat exchangers, fans/blowers, burner etc. The power conditioning system may include the inverter, converters, batteries etc. In addition to this, there is the air management system which may include a compressor, turbine, heat exchangers, fan, motor, etc. Furthermore, there are the Pumps, fans, compressors and blowers which faciltate the fuel and air supply in the system.
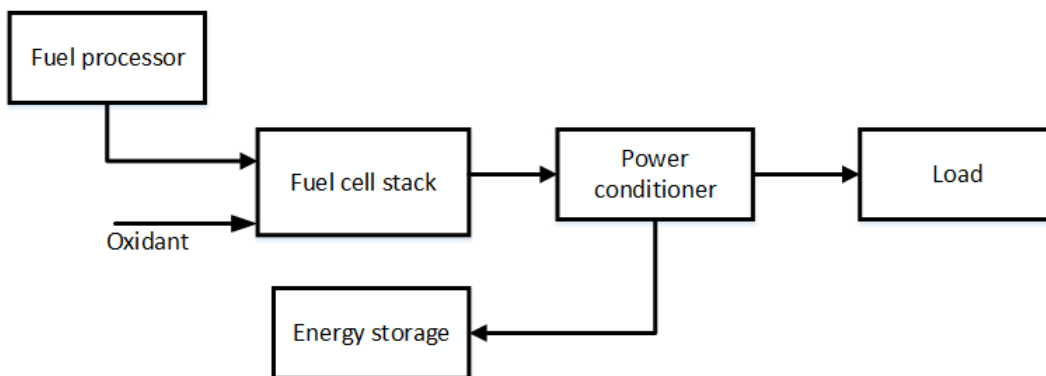

Figure 1.4. The Fuel cell power system organization, Diong [2010b].

The Figure 1.4 shows the system organisation through which the methanol is converted to the electricity. First the fuel (Methanol) is supplied to the tank, and the methanol leads to the reformer where it is mixed with water and this combination results to the hydrogen (H_2) and the carbon dioxide (CO_2). The electrochemical reaction that occurs in this process can be seen in equation 1.1.

$$CH_3OH_{(g)} + H_2O_{(g)} \longrightarrow CO_2 + 3H_2 \tag{1.1}$$

After that, the hydrogen (H_2) is fed to the fuel cell which normally consists of two electodes(anode and cathode) and an electrolyte layer. The hydrogen leads to the anode, where with the help of catalyst, it is separated into the protons (H^+) and the lectrons (e^-) as shown in equation 1.2, [Diong [2010a]]. The protons moves through the electrolyte layer to the cathode, and the electrons moves through the external circuit in order to reach the cathode side. As the oxygen (O_2) in the air moves to the cathodes, it is combined with the protons and electrons and form water. The electrochemical reaction that ocurrs under this process can be seen in equation 1.3.
The electrochemical reaction that takes place at anode side:

$$2H_2 \longrightarrow 4H^+ + 4e^- \tag{1.2}$$

The electrochemical reaction that takes place at cathode side:

$$O_2 + 4e^- + 4H^+ \longrightarrow 2H_2O \tag{1.3}$$

The figure 1.5 shows the basic workings of a fuel cell.
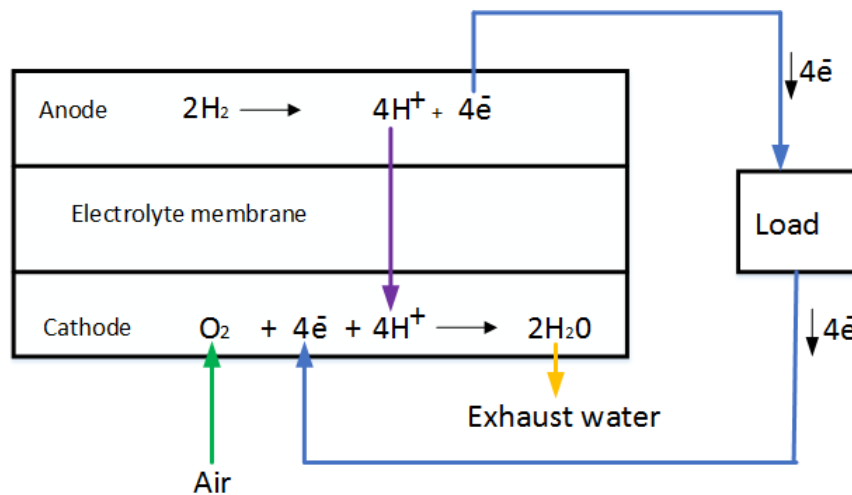

Figure 1.5. The physical structure of a fuel cell

From the Figure 1.5, the blue line represents the movement of the electrons through the external circuit, the green line represents the movement of oxygen in the air from surrounding, the dark purple represents the movement of the protons through the electrolyte membrane and the orange line represents the movement of the exhaust water.

The Balance of Plant components (BOP) for fuel cell like blowers, pumps and electronic controller are supplied with the voltage of $24V$ to be able to operate. Therefore, the buck conveter is used to convert the available voltage from fuel cell of the range $[38 - 70]$V to the needed voltage $[24]$V by BOP components. In the Figure 1.6, there can be seen the change behaviour of the generated cell voltage and power as a function of the cell current.
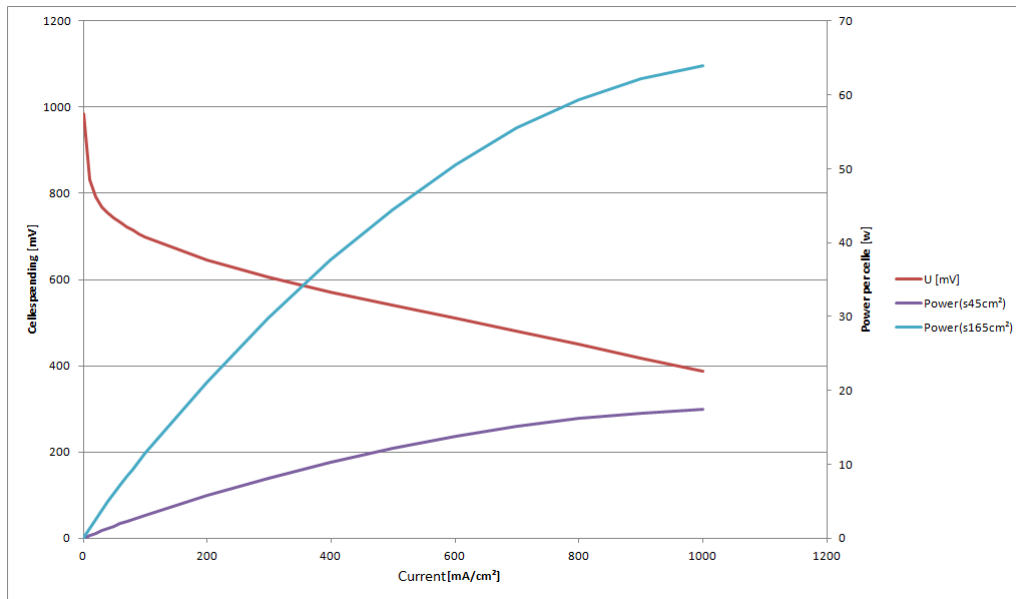
Figure 1.6. The generated voltage and power as a function of current in a fuel cell

From the Figure 1.6, the red line represents the generated cell voltage, the purple line represents the generated power of a cell with 45cm^2, and the light blue line represents the generated power of cell with 165cm^2 of surface area.

The required maximum power for the mentioned BOP components above (i.e Blowers, pumps and electroninic controller) is 400W. Therefore, in this project, it is desired to design a buck converter that meets the requirements which are the input voltage within the range $[38 - 70]$, the output voltage of 24V and the maximumum output power of 400W. In addition, the suitable controller will be designed to maintain the output voltage constant.

Buck converter analysis and Design

2

A DC/DC buck converter is needed to supply the required DC voltage by different equipments in the Fuel cell system. This chapter will explain the operating principle of DC/DC buck converter, then the buck converter will be designed.

2.1   Working principle of a DC/DC buck converter

The DC/DC buck converter is used to lower the input voltage. As shown in Figure 2.1, the buck converter consists of two semiconductors which can be either one transistor and one diode or two transistors to control the input voltage, one inductor to store the energy and capacitor to reduce the voltage ripple.
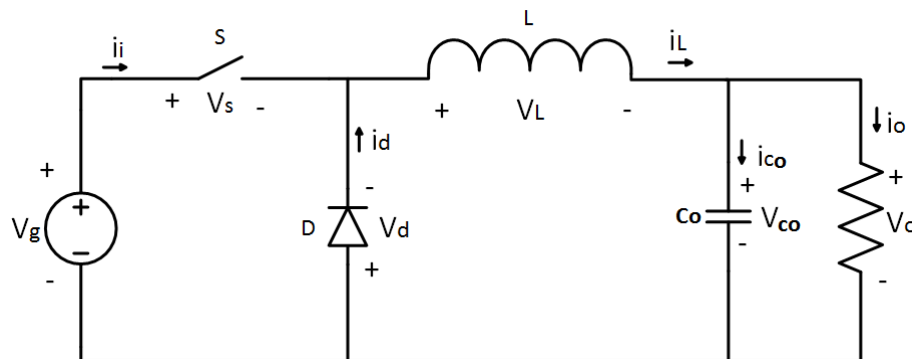

Figure 2.1. Circuit diagram of buck converter

The transistor device S in Figure 2.1 controls the input supply by being turned on and off periodically. The behaviour of the buck converter during the on and off-state of transistor S is described below:

On-state transistor: During this state, the inductor and capacitor are being charged by the input supply, and the diode is reverse biased i.e. there is no current flowing through it. The resulted equivalent circuit is shown in figure below:
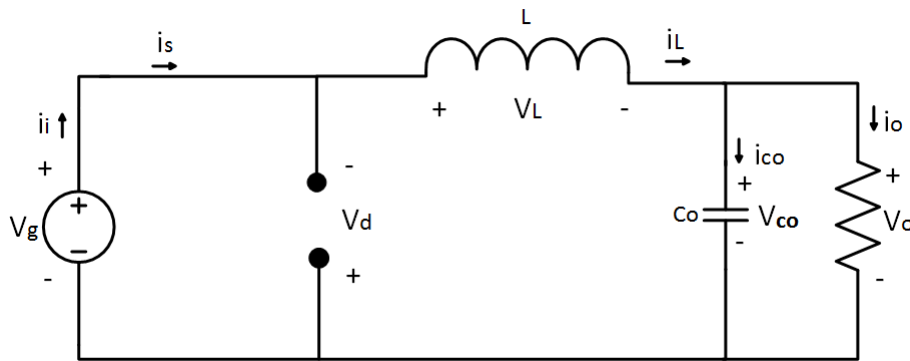
Figure 2.2. On-state circuit diagram of buck converter

During this state, the voltage through the inductor becomes $V_g - V_o$, thus as it can bee seen in the Figure 2.4 between the periode 0 and DT_s, the current through the inductor increases linearly with the positive slope given in equation 2.1, Maksimovic [2012a].

$$\frac{di_L(t)}{dt} = \frac{V_g - V_o}{L} \tag{2.1}$$

Off-state transistor: During this state, the inductor is charging the load, while the transistor S is opened, i.e. there is no current flowing through it. The resulted equivalent circuit diagram is shown in Figure 2.3.
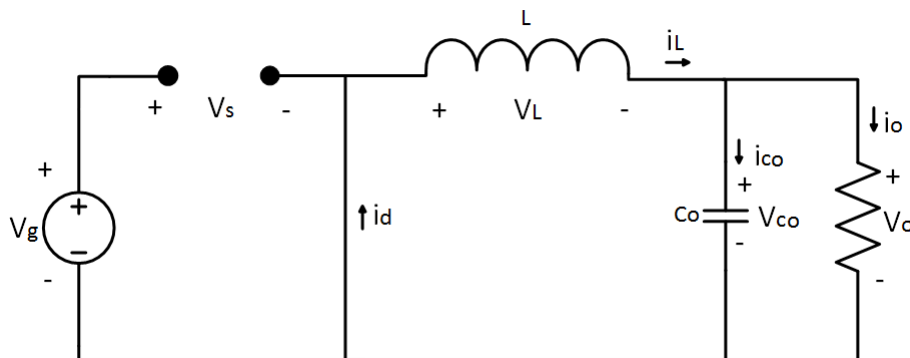

Figure 2.3. Off-state circuit diagram of buck converter

When the transistor S is turned off, the voltage in inductor becomes $-V_o$, therefore as it is shown in the Figure 2.4 between the periode DT_s and T_s, the current through the inductor starts to decrease linearly with slope given in equation 2.2, Maksimovic [2012b].

$$\frac{di_L(t)}{dt} = \frac{-V_o}{L} \tag{2.2}$$

There are two possible operation modes when dealing with DC/DC converter:

- **Continuous Conduction Mode (CCM)**: This occurs when the current through the inductor is always greater than 0 (i.e. $i_L > 0$) as it is shown in Figure 2.4
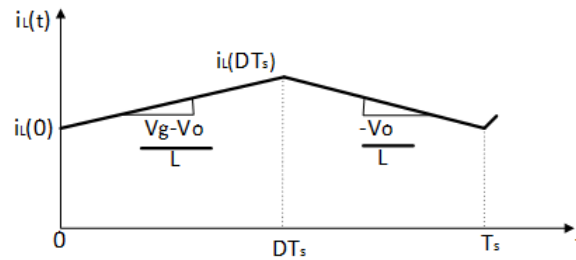
Figure 2.4. The inductor current waveform during CCM operation

- **Discontinuous Conduction Mode (DCM)**: In this situation, the current through the inductor reaches 0 during the off-state of transitor. From Figure 2.5, the indcuctor current is seen to be zero during the subinterval periode $[(D+D_1)T_s - T_s]$ before the end of cycle.
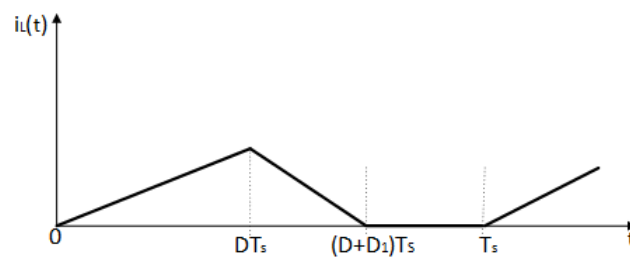

Figure 2.5. The inductor current waveform during DCM operation

In order to decide the proper size of each component of converter, it is very important to know in which mode the converter is working. This can be achieved by using the boundary between both mode(CCM and DCM).

The Figure 2.6 shows how the inductor current drops with reduction of the load current.

The average current through inductor $I_{o,lim}$ is seen to be less than $I_{o,2}$ which is also less than $I_{o,1}$. The boundary between both modes can only be found when the minimum of inductor current is zero which is seen to occur with the average inductor current $I_{o,lim}$ as it can be seen in Figure 2.6. Therefore $I_{o,lim}$ is considered to be the boundary between CCM and DCM.
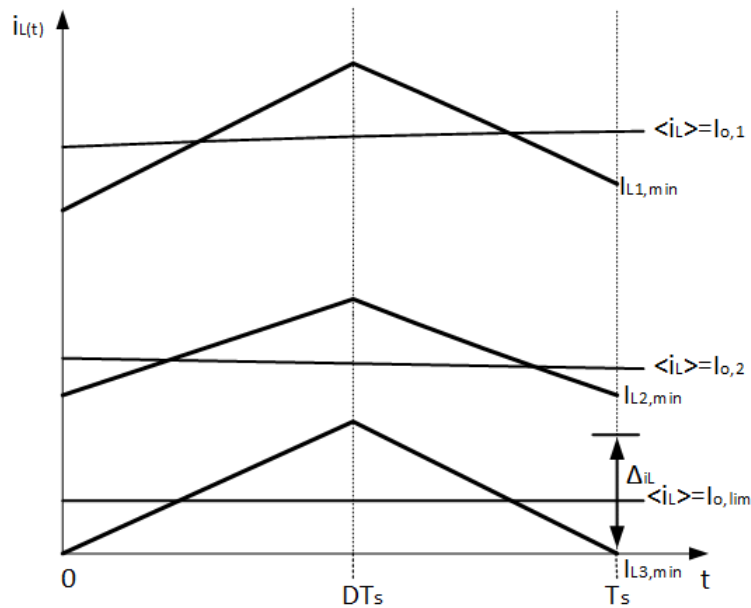
Figure 2.6. Inductor current waveform with different load current

If the output load current I_o becomes less than the boundary current $I_{o,lim}$, the inductor current will remain 0 and enters discontinuous mode as it was shown in Figure 2.5.

The boundary $I_{o,lim}$ (limit current) is equivalent to a half of the inductor current ripple $(\frac{\Delta iL}{2})$ and can be expressed in equation 2.3, Robert W.Erickson [2012].

$$I_{o,lim} = \frac{V_g T_s}{2L}(1-D)D \qquad (2.3)$$

For converter to operate in CCM, the output current I_o must be greater than the boundary $I_{o,lim}$, and to be operating in DCM, the output current I_o must be less than the boundary $I_{o,lim}$ ($I_o < I_{o,lim}$). From equation 2.3, it is seen that the higher inductance will reduce the ripple current in inductor, and this will make the converter operate in continuous mode. On the other hand, the higher load resistance will decrease the output load current, thus the convertert risks to enter the discontinuous mode as it is shown in Figure 2.6.
Comparing both operation modes, the continuous conduction mode (CCM) has the low peak current stress, and this reduces the power loss in the inductor, Mosfet and diode of converter. In addtion, the converter operating in CCM has low ripple current. Based on these factors, the Continuous Conduction Mode is chosen as the suitable operation mode for buck converter.

2.2   Power Losses analysis

As in other DC/DCC converter, the buck converter experiences the power loss in the components. These losses include the conduction losses and switching losses.

2.2.1   Conduction losses

Conduction losses occur due to the resistance in component and the forward voltage in semiconductors like a diode. Among those, there are:

- Mosfet conduction losses occur due to the on-resistance when the transistor is turned on, and this can be expressed as in equation 2.4

$$P_{sw(on)} = R_{Ds(on)}I_{L,RMS}^2 D + V_{Fsw} < i_{sw} > \qquad (2.4)$$

- Diode conduction losses occur due to the forward voltage when the diode is turned on. This can be found using the equation 2.5

$$P_D = V_{FD}I_{L,(off)}(1-D) + R_D I_{D,RMS}^2 \qquad (2.5)$$

- Capacitor conduction losses occur due to the Equivalent Series Resistance(ESR) of capacitors. The capacitor conduction loss can be found by:

$$P_{Co} = \frac{\Delta I_L^2}{12}R_{Co} \qquad (2.6)$$

- Inductor conduction losses occur due to the ESR of inductors. It ca be calculated from the expression:

$$P_L = (I_o^2 + \frac{\Delta I_L^2}{12})R_L \qquad (2.7)$$

2.2.2 Switching losses

Some power is consumed during the switching transition, since it takes moment for MOSFET and diode to change from on-state to off-state and vice versa. The Figure 2.7(a) shows the current and voltage behaviour in MOSFET, where $t_{sw,on}$ and $t_{sw,off}$ represent the voltage and current transitions periode.
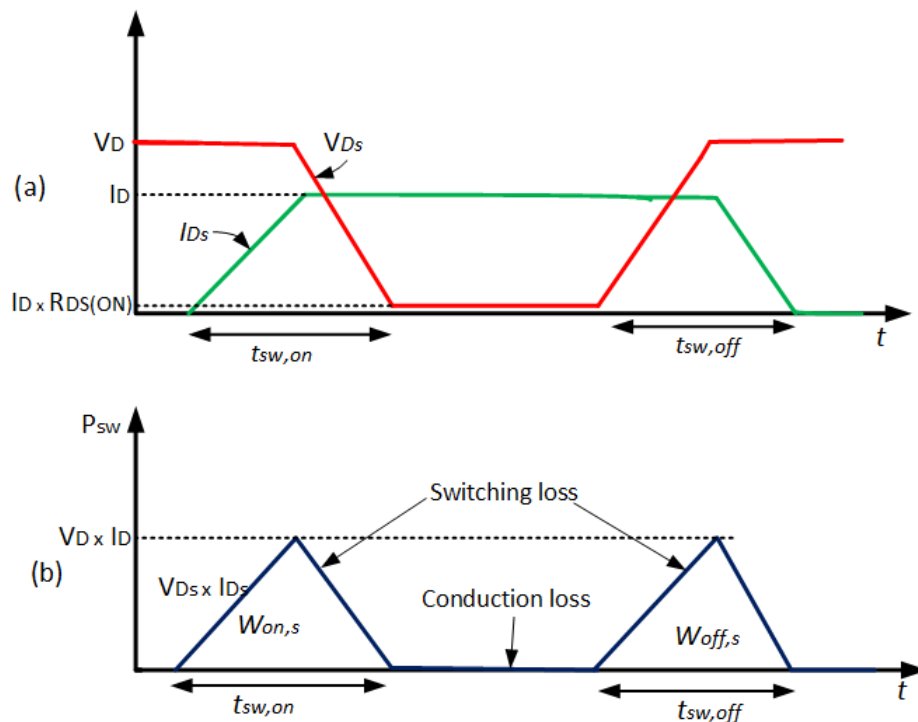

Figure 2.7. Switching losses during transistor transition between its on and off sate

From Figure 2.7 (a), During the on-state transition, the voltage V_{Ds} starts to decrease after that the current I_{Ds} has reached its full load current (I_D); and during the off-state transition, the current I_{Ds} starts to decrease when the voltage V_{Ds} has reached its final off-state value V_D.

Then, the lost power during these transitions is plotted in Figure 2.7 (b).

This switching loss in Mosfet can be found using the expression 2.8; Maksimovic [2012e].

$$P_{sw} = \frac{1}{2}V_D I_D(t_{sw,on} + t_{sw,off})f_s \qquad (2.8)$$

Where V_D is the drain to source voltage during the off state of Mosfet, I_D is the current during the on-state of Mosfet, f_s is the switching frequency, $t_{sw,on}$ is the turn-on transistion time and $t_{sw,off}$ is the turn-off transition time.

2.3 Converter Design

In this section, the buck converter is to be designed in order to determine each component's size.

Based on the information given in the first chapter, the following requirements and specifications are gathered in table 2.1.

Name	Operation range
Input voltage range	$V_i = [38;70]\text{V}$
Output voltage range	$V_o = 24\text{V}$
Maximum Output power	$P_{omax} = 400\text{W}$
Output current range	$I_o = [0.5;16]\text{A}$
Switching frequency	$f_s = [10;600]\text{kHz}$
Maximum output voltage ripple	$\Delta \widehat{V}_o < 1\% \cdot \widehat{V}_o$
Maximum inductor current ripple	$\Delta \widehat{i}_L < 30\% \cdot \langle i_{Lmax} \rangle$

Table 2.1. The requirements and specifications for design

The design below is for the buck converter operating in Continuous Conduction mode(CCM).

Duty cycle:

The Duty cycle for buck converter in continuous mode is defined as the voltage ratio between the output voltage and input voltage and its minimum and maximum value can be found using equation 2.9 and 2.10.

$$D_{min} = \frac{V_{o,min}}{V_{i,max}} = 0.34 \tag{2.9}$$

$$D_{max} = \frac{V_{o,max}}{V_{i,min}} = 0.63 \tag{2.10}$$

Maximumum and average current:

For buck converter, the maximum current in the inductor is the same as the maximum current in the switch, and these are obtained from the output current and inductor ripple current as shown in below equation 2.11:

$$I_{L,max} = I_{s,max} = I_{o,max} + \frac{\Delta i_{L,max}}{2} = 16.45A \tag{2.11}$$

The average current in the inductor is the same as the output current, thus the maximum and minimum average currrent are calculated from equation 2.12 and 2.13.

$$\langle i_{L,max} \rangle = I_{o,max} = 16A \tag{2.12}$$

$$\langle i_{L,min} \rangle = I_{o,min} = 0.5A \tag{2.13}$$

The average current in the switch depends on both duty cycle and output current, thus switch's maximum and minimum average current are found from equation 2.14 and 2.15.

$$\langle i_{s,max} \rangle = I_{o,max}D_{max} = 10A \tag{2.14}$$

$$\langle i_{s,min} \rangle = I_{o,min}D_{min} = 0.17A \tag{2.15}$$

Inductor selection

When designing the buck converter operating in CCM, the inductor size can be obtained by using the expressions shown in equation 2.16 and 2.17, Bidoggia [2014b].

$$L_1 = \frac{1}{2f_s} \frac{V_{o,max}}{I_{o,min}} \cdot (1 - \frac{V_{o,max}}{V_{i,max}}) \tag{2.16}$$

$$L_2 = \frac{1}{f_s \Delta i_{L,max}} \cdot V_{o,max}(1 - \frac{V_{o,max}}{V_{i,max}}) \tag{2.17}$$

Where the inductor value has to be greater than both L_1 and L_2.

$$L > max\{L1, L2\} \tag{2.18}$$

In the equation 2.16 and 2.17, it is found that the inductor size depends on the switching frequency which is given in range, $f_s = [10; 600]$kHz. In order to get the idea of how the inductance behaves with change of frequency, the estimated minimum inductance was plottet in Figure 2.8.
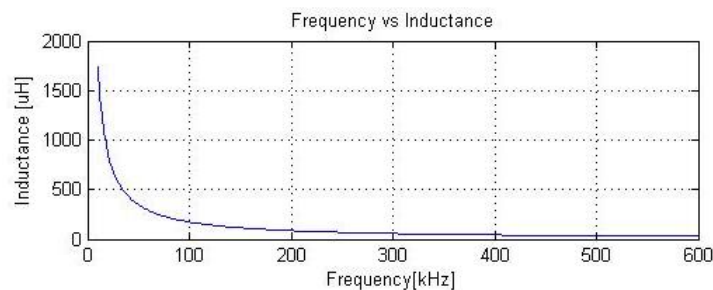

Figure 2.8. Change of inductance as a function of frequency

Output capacitor selection

The output capacitor serves as the filter for the DC/DC buck converter, where it reduces the output voltage ripple and overshoot.
The expression in equation 2.19 is going to be used to find out the minimum size for the output capacitor, Bidoggia [2014a].

$$C_o > \frac{\beta}{1 - \varepsilon_C} \cdot \frac{1}{8f_s \Delta \widehat{V_o}} \Delta \widehat{i_L} \tag{2.19}$$

Where β is the capacitor lifetime roundup and is about 1.2, ε_C is the capacitor tolerance and is about 0.2, f_s is the switching frequency, $\Delta \widehat{i_{L,max}}$ is the maximum inductor current ripple, and $\Delta \widehat{v_{o,max}}$ is the maximum output voltage ripple.
In the equation 2.19, it is seen that the capacitor size also depends on the switching frequency.
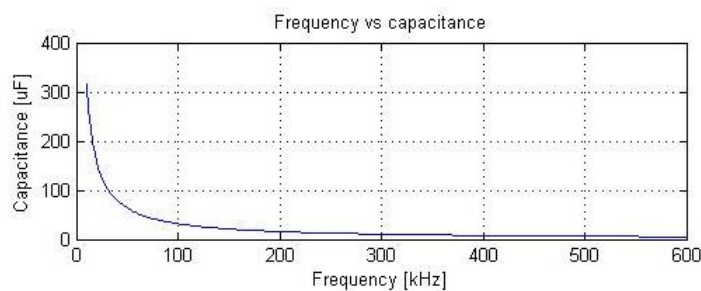The figure 2.9 shows the plot of the capacitance with change of the switching frequency.

Figure 2.9. Change of the capacitance as a function of frequency

In order to choose the suitable operating frequency, different factors are taken into consideration like the switching power loss, the size of inductor and capacitor. According to the equation 2.8, it can be seen that the low frequency will reduce the switching power loss. However, the low switching frequency will require a large size of the inductance and capacitance as it is shown in Figure 2.8 and 2.9. Based on theses factors, the suitable operating switching frequency is chosen to be 250kHz, then the inductor value is calcualted as 69μH, and the minimum capacitor value is calculated as 12.6μF. From these calculated values and the simulation results, the suitable inductance is chosen to be 69μH, and the suitable capacitance is chosen as 300μF as it is shown in Table 2.2.

-	Designed value	Chosen value
Inductance [μH]	L= 69	69
Capacitance [μF]	$C_o > 12.6$	300

Table 2.2. The chosen values of both inductor and capacitor

Controller analysis and Design

3

To keep the output voltage of converter constant, it is needed to include the controller into the system.

This chapter will include the dynamic model of switching buck converter, and then the controller will be designed. The type of control mode that is going to be used in this case is the current mode control. The main difference between the current mode control and voltage mode control is that for the current mode control, the error signal is used to directly control the peak transistor switch current, while for the voltage mode control, the error signal is compared to the constant ramp waveform to control the duty cycle [Maksimovic [2012c]].

However, there exist different type of current mode control such as the peak current mode control, valley current mode control, constant on-time current mode control, etc.

In this case, the LTC3810 is going to be used, and it uses the constant on-time control to ensure that the output voltage is fixed. The Figure 3.1 indicates the block diagram of a current mode converter that includes the inner current loop and outer voltage feedback loop.

3.1 Current Mode controller

As it can be seen in Figure 3.1, the diode which normally works as the passive switch is replaced by a synchronous MOSFET for better efficiency, then the on-resistor $(R_{DS(ON)})$ is used as a sense resistor for determining the inductor current signal.
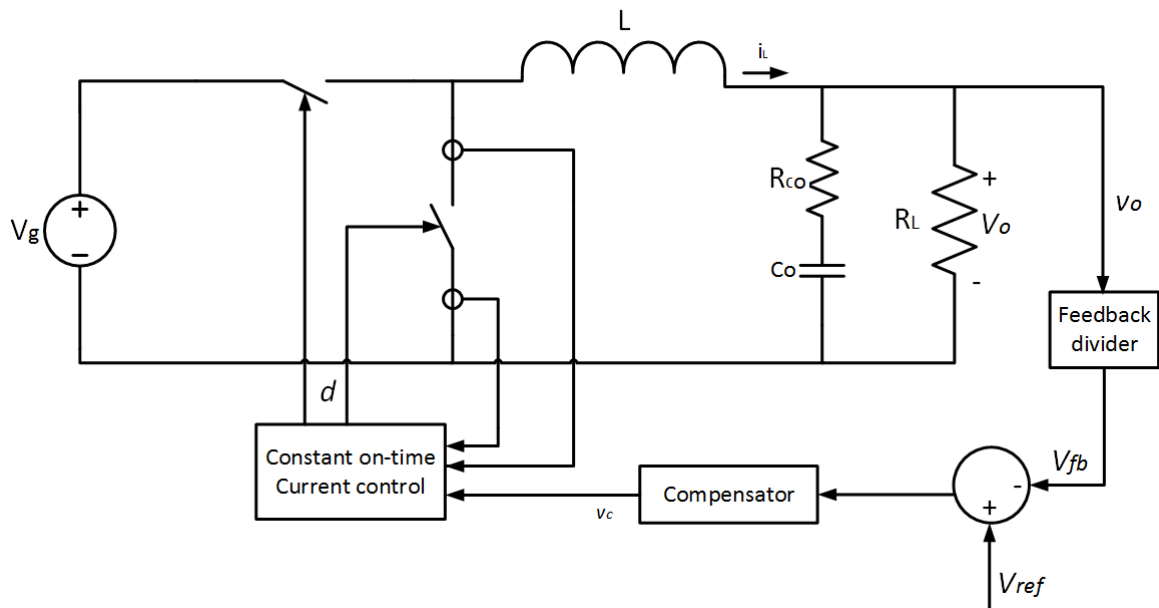

Figure 3.1. The buck converter diagram with current mode control circuit system

Where v_c is defined as the control signal.

In order to design the control system of buck converter, it is first needed to model the converter. Thus, in the next section, the average and small signal linear model of CCM buck converter are going to be developped using linearisation methode to derive the transfer functions.

3.2 Small signal modelling of buck converter with constant on-time current mode control

In order to find the control to output voltage transfer function, the control to inductor current transfer function will first be derived by applying a small sinusoidal perturbation on the control signal v_c, as it can be seen in Figure 3.2; and this will lead to the perturbed inductor current and PWM waveforms shown in figure 3.3.
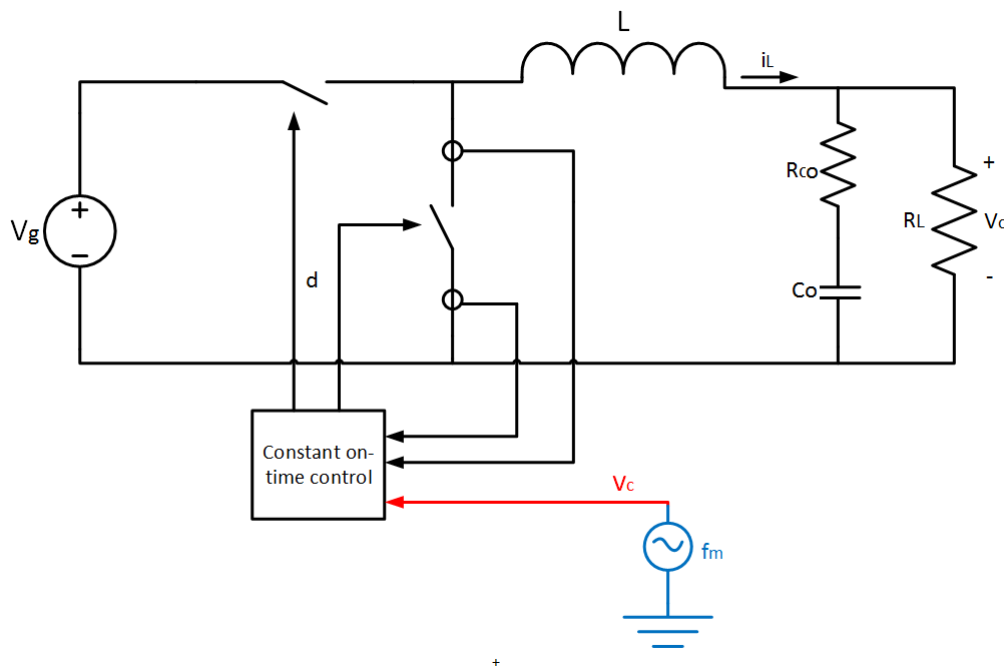

Figure 3.2. The equivalent circuit model with the applied small sinusoidal perturbation at frequency f_m
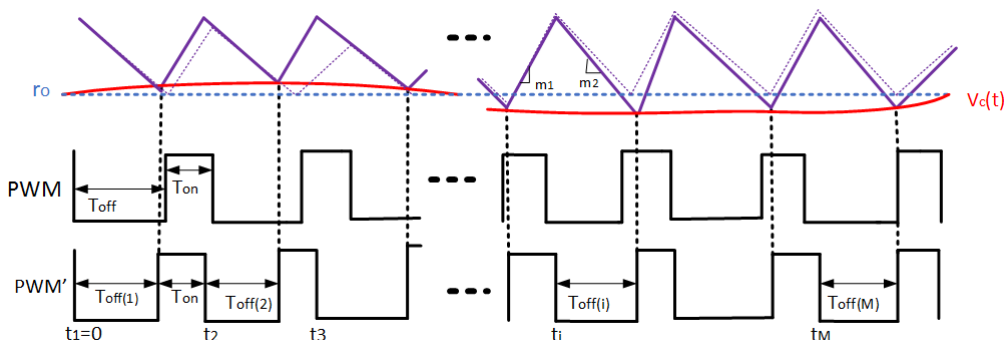

Figure 3.3. The inductor current waveform in constant on-time control

PWM represents the steady state PWM waveform, then PWM' represents the perturbed PWM waveform. Before starting with model derivation, it can be assumed that:

- The magnitude of the pertubation signal is very small
- The perturbation frequency f_m and the switching frequency f_s are defined by the relation:

$$N \cdot f_s = M \cdot f_m \tag{3.1}$$

where, N and M are positive integers.

Now the control to inductor transfer function is going to be derived by analysing the waveforms in Figure 3.3.

In the case of constant on-time current control, the on-time is constant, thus the off-time can be modulated by the perturbed signal as shown in equation 3.2

$$v_c(t) = r_o + \widehat{r} sin(2\pi f_m t - \theta) \tag{3.2}$$

Where, $v_c(t)$ is the perturbation signal, r_o is the steady state value of the control signal, $\widehat{r}$ is the magnitude of the signal, and θ is the initial angle. Now, the equation 3.3 can be found based on the modulation law:

$$v_c(t_{i-1} + T_{off(i-1)}) + m_1 T_{on} = v_c(t_i + T_{off(i)}) + m_2 T_{off(i)} \tag{3.3}$$

Where $T_{off(i)}$ is the i_{th} cycle off-time. Assuming that the perturbed off-time

$$T_{off(i)} = T_{off} + \Delta T_{off(i)} \tag{3.4}$$

Where the T_{off} is the steady-state off-time, and $\Delta T_{off(i)}$ is the difference between the perturbed i_{th} cycle off-time $T_{off(i)}$ and the steady-state off-time T_{off}. t_i can be defined as:

$$t_i = (i-1)(T_{on} + T_{off}) + \sum_{k=1}^{i-1} \Delta T_{off(k)} \tag{3.5}$$

Now $\Delta T_{off(i)}$ can be found from equation 3.3 as it is shown in below equation:

$$m_2 \Delta T_{off(i)} = v_c(t_{i-1} + T_{off(i-1)}) - v_c(t_i + T_{off(i)}) \tag{3.6}$$

Therefore, $\Delta T_{off(i)}$ becomes:

$$\begin{aligned}
\Delta T_{off(i)} &= \frac{1}{m_2} \widehat{r} \{ sin[2\pi f_m \cdot (t_{i-1} + T_{off(i-1)}) - \theta] - sin[2\pi f_m \cdot (t_i + T_{off(i)}) - \theta] \} \\
&\approx -\frac{1}{m_2} \widehat{r} \cdot 2cos[\pi f_m \cdot (t_{i-1} + t_i + 2T_{off}) - \theta] \cdot sin(\pi f_{mT_{sw}}) \\
&\approx -2\frac{1}{m_2} \widehat{r} \cdot sin[\pi f_m \cdot (T_{on} + T_{off})] \cdot cos[2\pi f_m(i-1)(T_{on} + T_{off}) - \frac{T_{on} - T_{off}}{2}]
\end{aligned} \tag{3.7}$$

The pertubed inductor current $i_L(t)$ can be defined in equation 3.8.

$$i_L(t)|_{0 \leq t \leq t_M + T_{off(M)} + T_{on}} = \int_0^t [\frac{V_i}{L} d(t)|_{0 \leq t \leq t_M + T_{off(M)} + T_{on}} - \frac{V_o}{L}] dt + i_{Lo} \tag{3.8}$$

The fourier analysis is going to be applied to the inductor current, and the resulted fourier coefficient of the inductor current $C_{m(iL)}$ at the perturbation frequency f_m is given in the equation 3.9.

$$C_{m(iL)} = -\frac{1}{N\pi} \frac{V_i}{L} e^{-j2\pi f_m T_{off}} (1 - e^{-j2\pi f_m T_{on}}) [\sum_{i=1}^{M} (e^{-j2\pi f_m(i-1)T_{sw}} \cdot \sum_{k=1}^{i} \Delta T_{off(k)})] \tag{3.9}$$

17

By insterting the equation 3.7 into equation 3.9, this will yield the expression given in 3.10.

$$C_{m(iL)} = \frac{V_i}{L \cdot j2\pi f_m} \hat{r} \frac{f_s}{m_2} (1 - e^{-j2\pi f_m T_{on}}) e^{-j\theta} \tag{3.10}$$

Now, the the transfer function from the control to the inductor current can be obtained as:

$$\frac{i_L(s)}{v_c(s)} = \frac{C_{m,L}}{\hat{r} \cdot e^{-j\theta}} = \frac{f_s}{m_2} \frac{V_i}{Ls} (1 - e^{-sT_{on}}) \tag{3.11}$$

where s is defined as $s = j2\pi f_m$.
Using the pade' approximation, the exponential term $e^{-sT_{on}}$ can be defined as shown in equation 3.12.

$$e^{-sT_{on}} = 1 - \frac{sT_{on}}{1 + \frac{s}{Q_1\omega_1} + \frac{s^2}{\omega_1^2}} \tag{3.12}$$

where $\omega_1 = \frac{\pi}{T_{on}}$ and $Q_1 = \frac{2}{\pi}$.

By substituting the equation 3.12 into 3.11, this will lead to the expression given in equation 3.13.

$$\frac{i_L(s)}{v_c(s)} \approx \frac{1}{R_i} \cdot \frac{1}{1 + \frac{s}{Q_1\omega_1} + \frac{s^2}{\omega_1^2}} \tag{3.13}$$

Using the circuit diagram in figure 3.1, the inductor current can also be expressed as function of output voltage through the equations 3.14.

$$\begin{aligned}
i_L(s) &= \frac{V_o(s)}{R_{co} + \frac{1}{sC_o}} + \frac{V_o(s)}{R_L} \\
&= \frac{V_o(s)R_L + V_o(s)(R_{co} + \frac{1}{sC_o})}{(R_{co} + \frac{1}{sC_o})R_L} \\
&= V_o(s)\frac{(1 + sR_{co}C_o)R_L}{(R_L + R_{co})sC_o + 1}
\end{aligned} \tag{3.14}$$

Finally, the control to outout transfer function can be obtained in equation 3.15.

$$\frac{v_o(s)}{v_c(s)} \approx \frac{1}{R_i} \cdot \frac{1}{1 + \frac{s}{Q_1\omega_1} + \frac{s^2}{\omega_1^2}} \cdot \frac{R_L(R_{co}C_o s + 1)}{(R_L + R_{co})C_o s + 1} \tag{3.15}$$

The derivation for the control to output transfer function in detail can be seen in appendix A.
The designed values of each component in circuit are listed in below table:

Name	Chosen value
Inductance [μH]	69
Capacitance [μF]	300
Duty cycle	0.53
Output voltage [V]	24
Reference voltage [V]	0.8
Resistance [Ω]	2
Switching frequency [kHz]	250
Switching time [μs]	4

Table 3.1. The chosen values of the converter compoennts

Using all these values in table 3.1 into the equation 3.15, the control to output transfer function becomes:

$$G_{vc}(s) = \frac{4.615 \cdot 10^{-4}s + 76.92}{2.76 \cdot 10^{-16}s^3 + 6.428 \cdot 10^{-10}s^2 + 6.07 \cdot 10^{-4}s + 1} \qquad (3.16)$$

3.3 Compensator Design

As the control to output transfer fucntion $G_{vc}(s)$ of the current mode controlled converter is determined in the last section, it is now needed to design a suitable compensator $G_c(s)$ to filter the error signal in order to keep the output voltage constant. The Figure 3.4 shows the block diagram of feedback system which includes the compensator $G_c(s)$, the current controlled converter $G_{vc}(s)$ and the sensor gain $H(s)$.
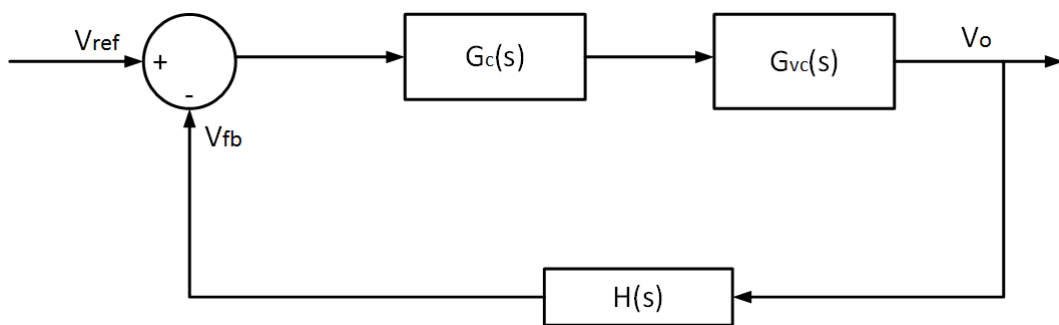

Figure 3.4. Block diagram of the system

In this section, it is going to design the proportional integral (PI) type-II compensator shown in Figure 3.5. This type-II compensator contains an integrator, one pole and one zero located between the integrator and pole. The schematic of the type-II compensator can be seen in the Figure 3.5.
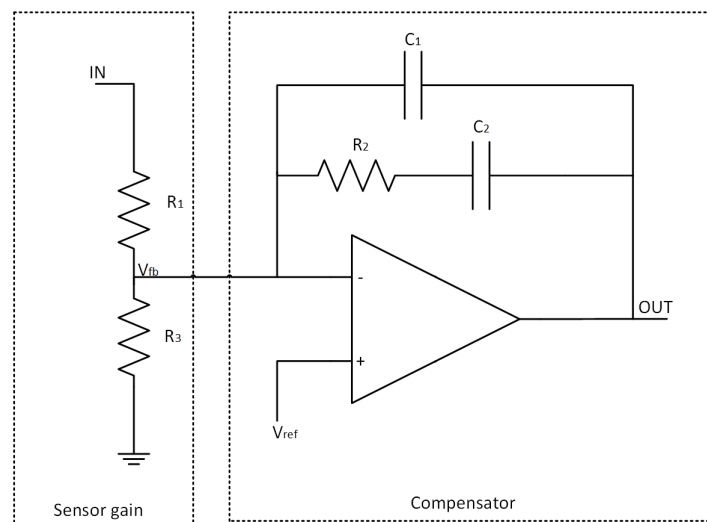

Figure 3.5. Circuit diagram of type-II compensator with feedback divider

Calculating the impedances in Figure 3.5, the transfer fucntion of the type II compensator is obtained in

equation 3.17.

$$G_c(s) = -\frac{K}{s}\frac{1+s\tau_1}{1+s\tau_2} \tag{3.17}$$

Where:

$$K = \frac{1}{R_1(C_1+C_2)}$$
$$\tau = R_2C_2 \tag{3.18}$$
$$\tau = R_2 \cdot \frac{C_1C_2}{C_1+C_2}$$

The component values of C_1, C_2, R_1, R_2 and R_3 will be determined. The component values of current mode controlled converter are given in Table 3.1. These values will be used to find the component values of the compensator shown in Figure 3.5. In the equation 3.2, it can be seen that the uncompensated converter control-to-output transfer function has one zero which can be calculated by setting the numerator to zero as it is shown in equation 3.19 , and the poles can be obtained by setting the denominator to zero as shown in equation 3.20.

$$4.615 \cdot 10^{-4}s + 76.92 = 0 \tag{3.19}$$

$$2.76 \cdot 10^{-16}s^3 + 6.428 \cdot 10^{-10}s^2 + 6.07 \cdot 10^{-4}s + 1 = 0 \tag{3.20}$$

From the above equation 3.19 and 3.20, it is found out that the transfer function $G_{vc}(s)$ has one zero located at frequency $f_z = 26.5\text{kHz}$ and three poles which are located at frequency : $f_{p,1} = 262.6\text{Hz}$; $f_{p,2} = 146 + j185.2\text{kHz}$ and $f_{p,3} = -146 + j185.2\text{kHz}$. In order to obtain the sufficient phase margin, the crossover frequency f_c of the system is chosen to be $\frac{1}{10}$ of the switching frequency.

$$f_c = \frac{f_s}{10} = 25kHz \tag{3.21}$$

To avoid a $-180°$ phase shift in the loop gain before the crossover frequency, the zero of the compensator is selected to be half lower than the converter's pole. However, in order to limit the phase margin degradation, the compensator pole is chosen to be five greater than the crossover frequency. The compensator zero and pole are calculated in equation 3.22

$$f_{c,zero} = \frac{f_{p,1}}{2} = 131.3Hz \qquad\qquad f_{c,pole} = 5f_c = 125kHz \tag{3.22}$$

The compensator gain can be calculated at crossover frequency, by the following expression:

$$|\,G_c(f_c)\,| = \frac{1}{|\,G_p(f_c)\,|} = 0.903 \tag{3.23}$$

In oder to find the component values of compensator, $C_2 = 45.3\text{n}$ is chosen as starting point, then the rest component values are calculated as below:

$$\tau_1 = \frac{1}{2\pi f_{c,zero}} = 12.12 \times 10^{-4} \tag{3.24}$$

$$\tau_2 = \frac{1}{2\pi f_{c,pole}} = 1.273 \times 10^{-6} \tag{3.25}$$

$$R_2 = \frac{\tau_1}{C_2} = 26.75k\Omega \tag{3.26}$$

$$C_1 = C_2\frac{\tau_2}{\tau_1 - \tau_2} = 47.6pF \tag{3.27}$$

$$R_1 = \left| \frac{G_p(f_c)}{2\pi f_c(C_1 + C_2)} \times \frac{1 + j2\pi f_c\tau_1}{1 + j2\pi f_c\tau_2} \right| = 29.02k\Omega \tag{3.28}$$

Now the resistance R_3 can be calculated from the output voltage $V_o = 24$ V , the resistance $R_1 = 2.98$ kΩ and the reference voltage $V_{ref} = 0.8$V as it is shown in the expression of equation 3.29:

$$R_3 = \frac{V_{ref}R_1}{V_o - V_{ref}} = 1k\Omega \tag{3.29}$$

The obtained values above are subsituted into equation 3.17, and this leads to the compensator transfer function in equation 3.30.

$$G_c(s) = -\frac{759.8(12.12 \times 10^{-4}s + 1)}{s(1.273 \times 10^{-6}s + 1)} \tag{3.30}$$

The frequency domain response of the current mode converter and compensator are shown in Figure 3.6.
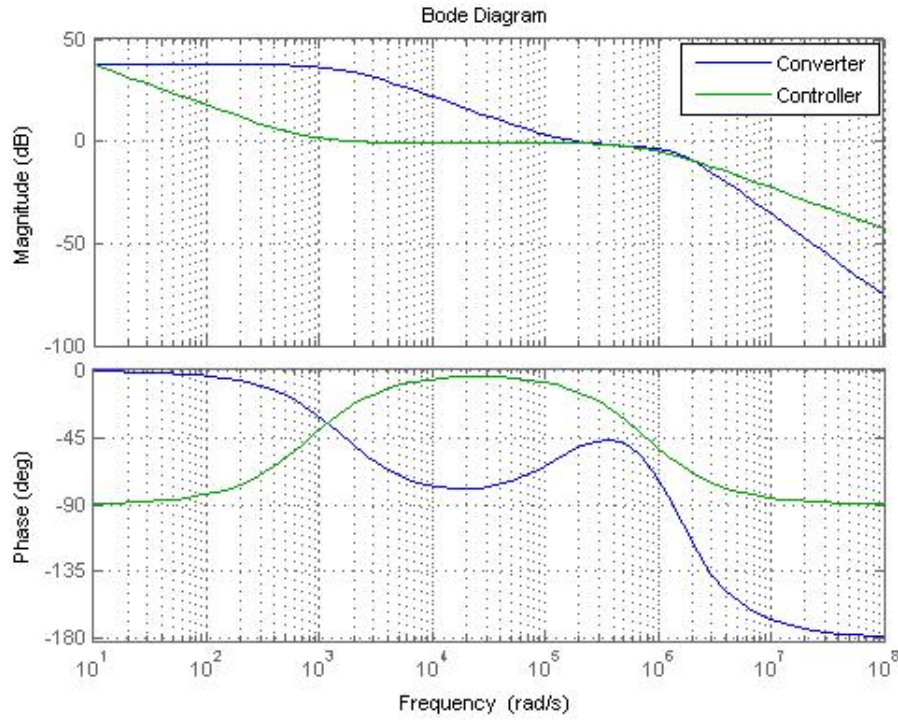

Figure 3.6. The bode plot of both current mode converter and type 2 compensator

The phase margin of the current mode converter is seen to be $128°$, and the gain margin is infinity because the phase never cross $-180°$.

The open loop transfer function for the system including the compensator is then obtained as:

$$G_{ol}(s) = \frac{1.417 \cdot 10^{-5}s^2 + 2.37s + 1948}{s(3.51 \times 10^{-22}s^4 + 1.09 \times 10^{-15}s^3 + 1.41 \times 10^{-9}s^2 + 6.08 \cdot 10^{-4}s + 1)} \tag{3.31}$$

The closed loop transfer function is determined in equation 3.32.

$$G_{cl}(s) = \frac{4.25 \cdot 10^{-4}s^2 + 71.19s + 5.84 \cdot 10^4}{3.51 \cdot 10^{-22}s^5 + 1.094 \cdot 10^{-15}s^4 + 1.41 \cdot 10^{-9}s^3 + 6.22 \cdot 10^{-4}s^2 + 3.37s + 1948} \tag{3.32}$$

Now, the frequency response of the compensated system can be seen in figure 3.7.
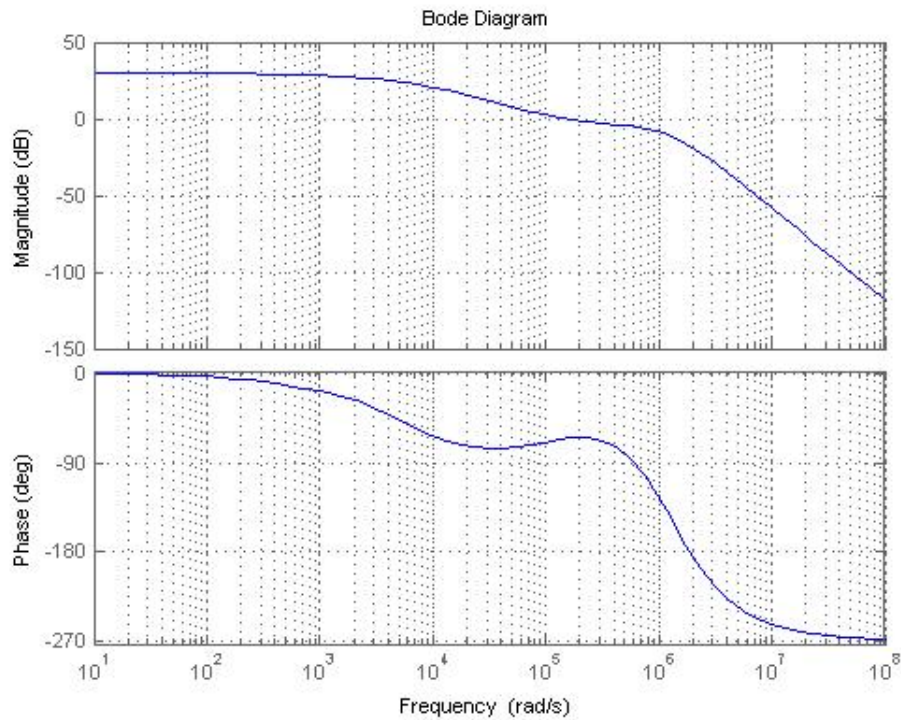

Figure 3.7. The compensated current mode converter

In the Figure 3.7, the gain margin reads 17.8 dB and the phase margin is read to be $114°$. it can also be seen that the compensated system crosses the 0db at crossover frequency $f_c = 154000\frac{rad}{s}$ at $-20deb/dec$, which is close to the expected crossover frequency of 25kHz.

To know the location of the compensated system poles, the root locus is used as shown in Figure 3.8. In that figure, it can be seen that all the poles for compensated system are found on the left half plane.
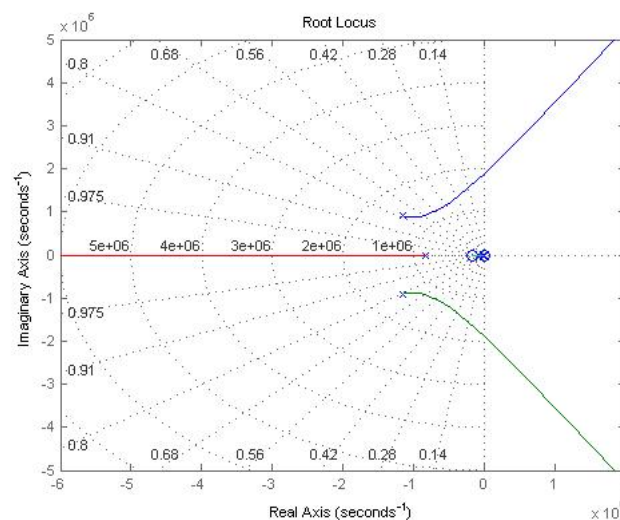

Figure 3.8. The root locus for the compensated system

From the Figure 3.8, the closed loop poles location are found to:

$-1.145 + j9.09 \cdot 10^5; -1.145 - j9.09 \cdot 10^5; -8.17 \cdot 10^5; -4823.15$ and -657.07.

As the closed loop poles are all located on the left half plane, and it has been found that there is only one crossover frequency at $f_c = 25$ kHz and the phase margin is determined as $114°$ which is positive, therefore it can be concluded that the closed loop system is stable, Maksimovic [2012d].

The step response for both compensated and uncompensated conevrter system can be seen in figure 3.9.
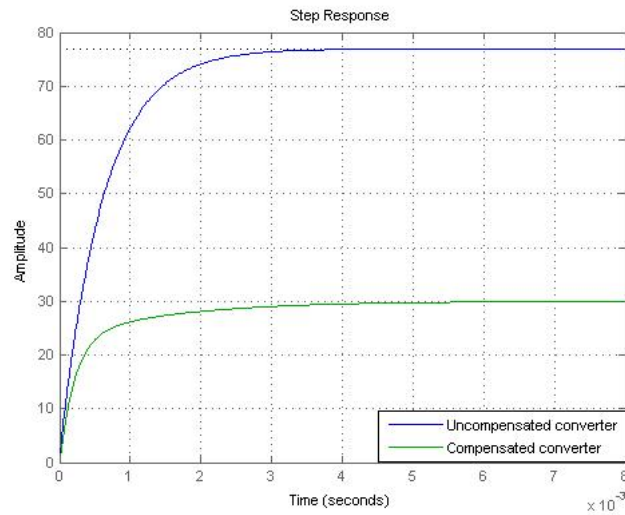

Figure 3.9. The step response for both compensated and uncompensated converter

It can be seen that for the uncompensated system, the peak amplitude is 76.9 which has been lowered to 30 for the compensated system.

Simulation of the whole schematic of Converter

4

In this chapter, the structure of converter system will be analysed based on the designed component values of the converter and controller in chaptter 2 and 3. Futhermore, the converter model will be simulated in LTspice software. The Figure 4.1 shows the converter schematic including the integrated circuit control LTC3810 and the compensator.
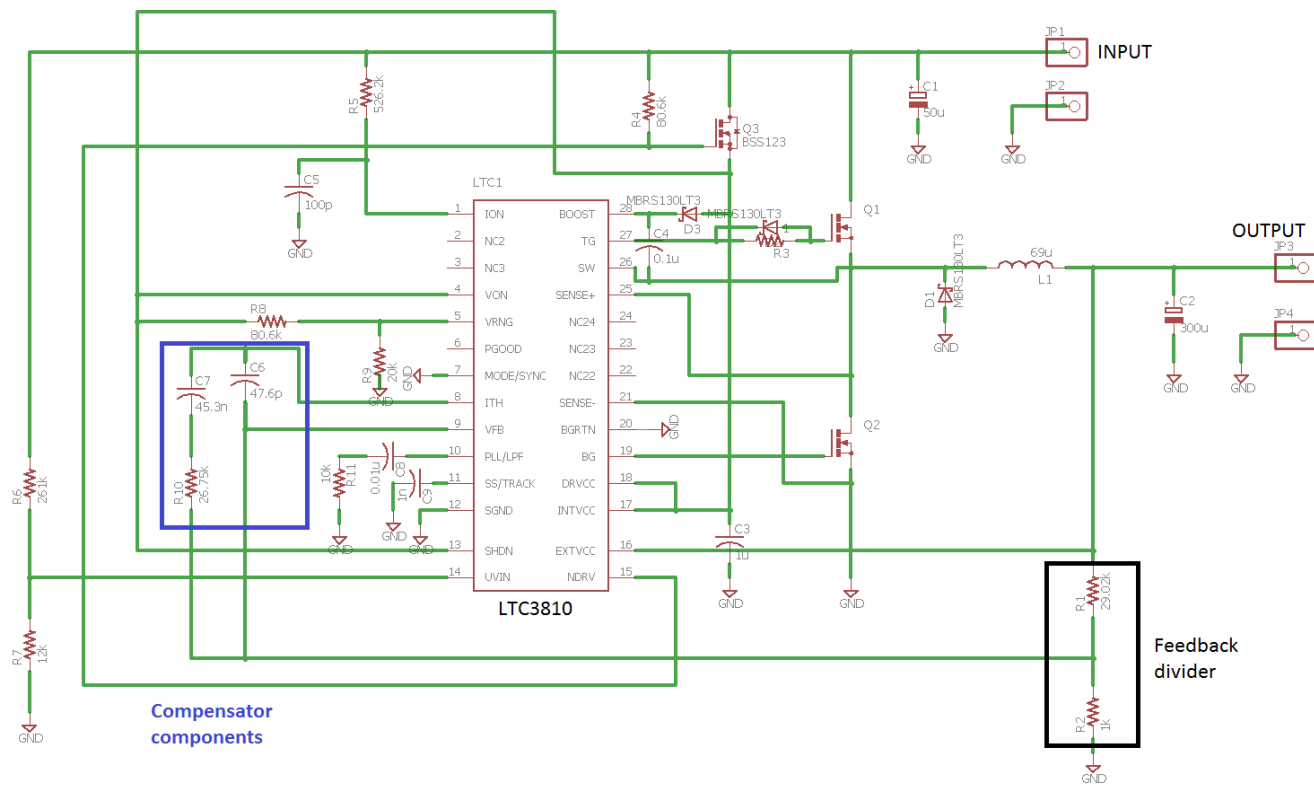

Figure 4.1. The whole schematic of the system

In Figure 4.1, the LTC3810 is the current mode synchronous switching controller which can operate with the input voltage up to $100V$, and it uses a constant on-time valley current controller [Lineartechnology [2007]]. As shown in figure 4.1, LTC3810 has 28 different pins. The Mosfet(Q_2) on-resistance serves as the sense resistor to determine the current through the inductor. The used MOSFETs Q_1 and Q_2 are Si7850DP of type N-channel fast switching mosfet

The components located in blue rectangle in figure 4.1 are the compensator components designed in the previous chapter.

In addition to this, there is the feedback divider in black rectangle, which is composed by 2 resistors which were also determined in the previous chapter in equations 3.28 and 3.29.

The used symbols of the compensator components in Figure 4.1 are different from those ones used in Figure 3.5, and their correspondance can be seen in table 4.1.

used symbols in Design —>	used symbols in schematic diagram
C_1 —>	C_6
C_2 —>	C_7
R_1 —>	R_1
R_2 —>	R_{10}
R_3 —>	R_2

Table 4.1. The correspondance between compensator symbol from design and the schematic diagram

Simulation

The compensated converter system presented in Figure 4.1 is simulated using Ltspice software as it is shown in Figure 4.2, and the simulation results of the inductor current and the output voltage waveforms can be seen in Figure 4.3 and 4.4.
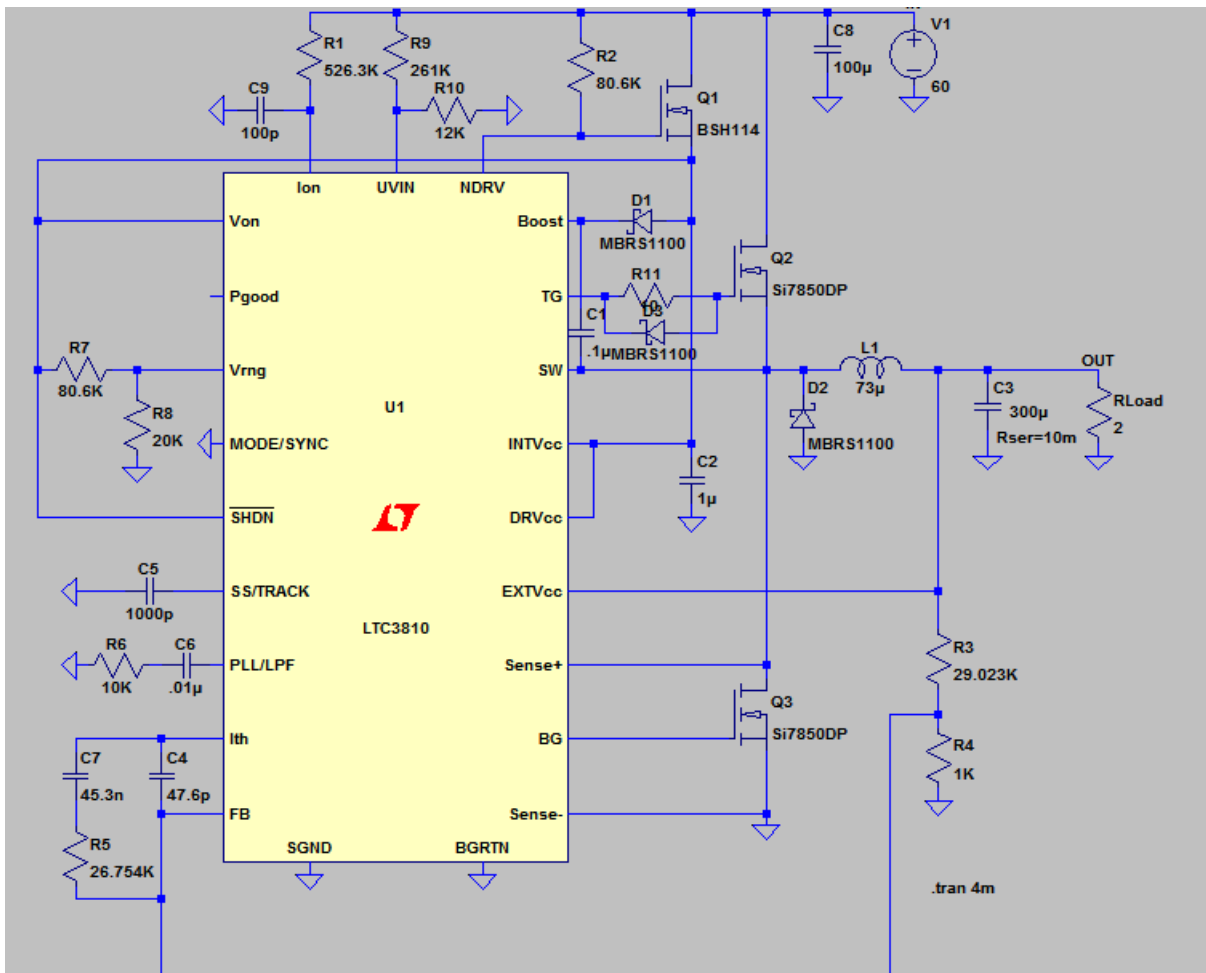

Figure 4.2. The simulation of the whole circuit digaram of system

According to the requirements given in Table 2.1, the desired output voltage is 24V and the allowed output

voltage ripple is expected to be less than 0.24V. Comparing to the results from the simulation in Figure 4.4, it can be seen that the output voltage ripple is very small, about 8mV.

Regarding the inductor current, the simulation results is shown in Figure 4.3, and it can be seen that the ripple current is about 0.82A which is less than the allowed maximum inductor current ripple which is 3.6A.
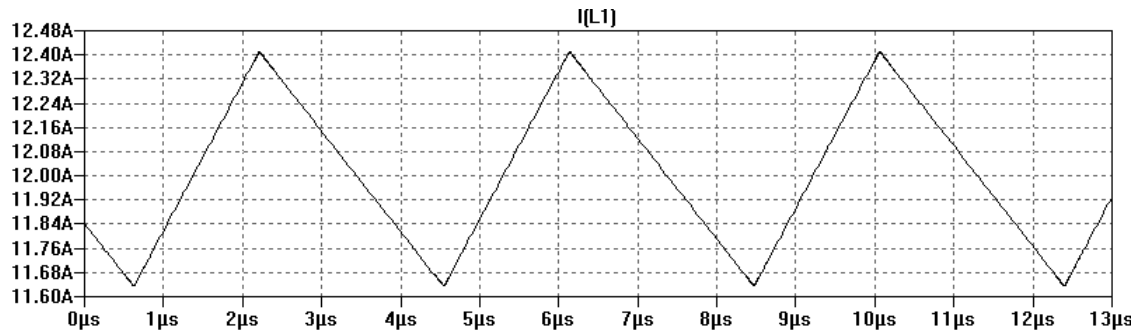

Figure 4.3. The simulated inductor current waveform with $V_i = 60V$ and $R_L = 2\Omega$
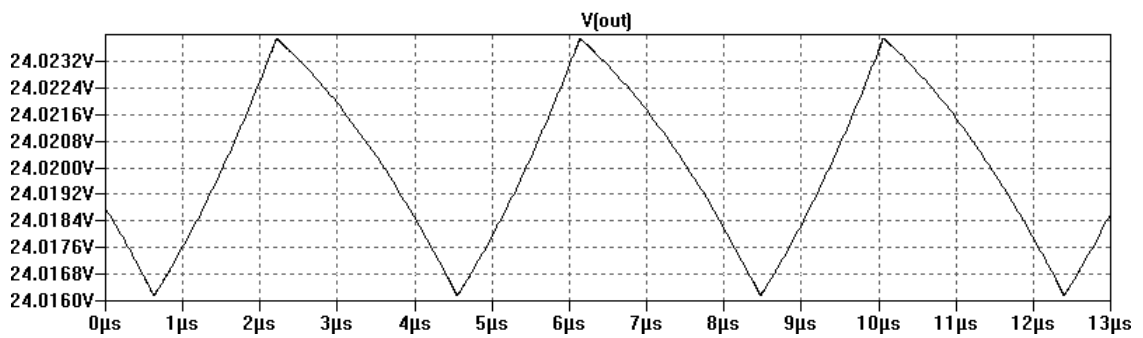

Figure 4.4. The simulated output voltage waveform

Conclusion and Future work 5

This chapter will give the conclusion for project and the future work.

The main goal of this project was to design a buck converter which is able to supply the 24V to the BOP components for fuel cell with a maximum output power of 400W. In addition, it was intended to design a compensator to maintain the output voltage constant.

Therefore, based on the required parameters given in Table 2.1, the buck converter was designed and the calculated component sizes are presented in Table 3.1.

Furthermore, the dynamic model for converter was carried out by applying a small sinusoidal perturbation on the control signal v_c, then the needed transfer function of the control to the output voltage was derived and obtained in equation 3.15.

In order to keep the output voltage constant, the compensator was needed to be included in the system, thus the type 2 compensator was designed, and the resulted transfer function is given in equation 3.30. To verify the behaviour and stability of the converter system with the controller, the matlab software was used by bode plotting the system with the controller as shown in Figure 3.7, where there is one crossover frequency of $15400\frac{rad}{s}$, which is close to 25kHz calculated in equation 3.21, and then all the poles are placed in the left halfplane as shown in Figure 3.8.

In addition, the simulation of the full circuit shown in Figure 4.1 was created in LTspice software in figure 4.2, where the inductor current ripple was found to be 0.8A which is less than the allowed maximum inductor current ripple. Then, the output voltage ripple was found to be very small around 8mV, which means that the output voltage is constant.

Future work:

The more accurate model is very important for the converter system when designing the feedback loop control. However, the dynamic model of constant on-time converter sytem has not taken into account everything like the input voltage etc. Therefore, in the future, it is needed to expand the simplification of the model, thereby considering the influence from the input voltage and output voltage.

Regarding the compensator, it could also be nice to investigate other type of controllers, so that their performance can be compared.

Furthermore, the pcb design should be improved by designing the PCB with 4 layers instead of 2 layers. The PCB with 4 layers has a better performance than 2 layers in terms of reducing the electromagnetic interface (EMI) and noise.

Bibliography

Benoit Bidoggia. Buck converter design in ccm(page. 2.38-2.39), 2014a. URL `https://dl.dropboxusercontent.com/u/21539584/notesDCDC/BidoggiaNotes-0-0-11-C.pdf`.

Benoit Bidoggia. Buck design procedure in ccm, (page. 2.34-2.35), 2014b. URL `https://dl.dropboxusercontent.com/u/21539584/notesDCDC/BidoggiaNotes-0-0-11-C.pdf`.

Bei Gou. Woon Ki Na. Bill Diong. *Fundamentals of fuel cells*, chapter 2, page 5. Boca raton, 2010a.

Bei Gou. Woon Ki Na. Bill Diong. *Fuel cells Modeling, Control, and Application*, chapter 1, page 3. Boca raton: CRC press, 2010b.

Energistyrelsen. Montly energy statistics, 2015. URL `https://ens.dk/service/statistik-data-noegletal-og-kort/maanedlig-og-aarlig-energistatistik`.

Lineartechnology. Current mode sycnronous switching regulator controller, 2007. URL `http://cds.linear.com/docs/en/datasheet/3810fc.pdf`.

R. W.Erickson; Dragan Maksimovic. *Principles of steady-state converter*, chapter 2, page 18. Ne, 2012a.

Robert W.Erickson; Dragan Maksimovic. *Principles of steady-state converter analysis*, chapter 2, page 18. New york, 2012b.

Robert W.Erickson; Dragan Maksimovic. *Current programmed control*, chapter 12, page 439. New, 2012c.

Robert W.Erickson; Dragan Maksimovic. *Stability*, chapter 9, page 342. New, 2012d.

Robert W.Erickson; Dragan Maksimovic. *Switching loss*, chapter 4, page 94. New york, 2012e.

; Dragan Maksimovic Robert W.Erickson. *Fundamentals of power electronics*, chapter 5, page 110. New, 2012.

Linear technology. Pin configuration, 2007. URL `http://cds.linear.com/docs/en/datasheet/3810fc.pdf`.

Derivation of Constant on-time control buck converter transfer function

A

In the Figure A.1, it can be seen that the small sinusoidal perturbation at frequency f_m is applied to the control signal v_c.
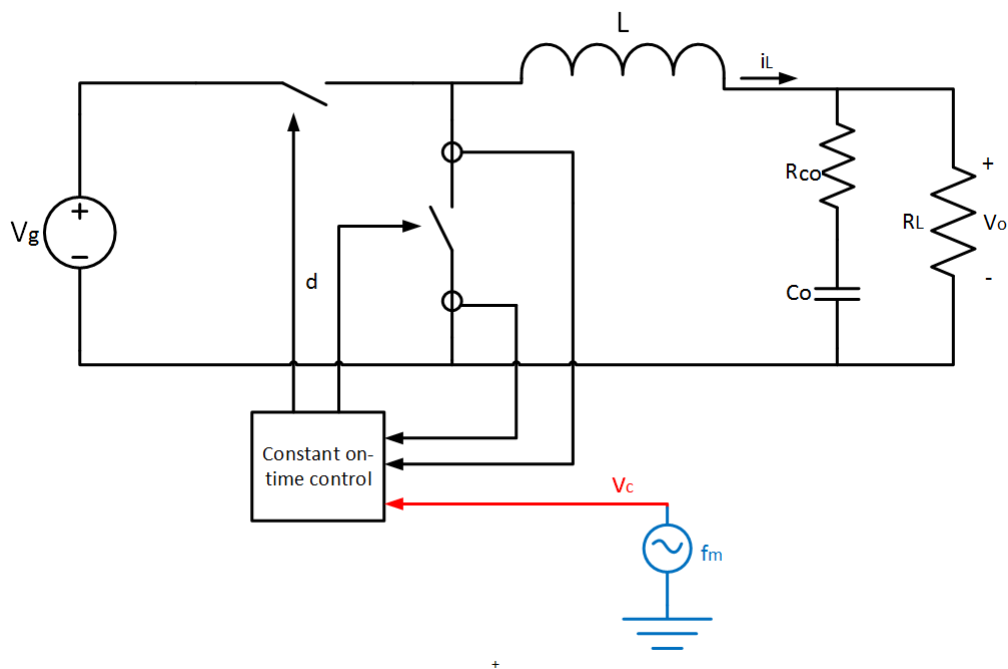

Figure A.1. The equivalent circuit modleing with the small sinusoidal perturbation applied on control signal v_c

In this case, the on-time is constant, thus the off-time will be modulated using that applied pertutbation signal.

$$v_c(t) = r_o + \widehat{r} sin(2\pi f_m t - \theta) \tag{A.1}$$

Where θ is the initial angle of the sinusoidal perturbation signal. It is assumed that the perturabtion frequency f_m and the switching frequency f_s relation is defined as in the equation A.2:

$$N f_s = M f_m \tag{A.2}$$

Where N and M are the positive integers.

The equation A.3 can be obtained according to the modulation law of constant on-time control as it is shown in Figure 3.3.

$$v_c(t_{i-1} + T_{off(i-1)}) + m_1 T_{on} = v_c(t_i + T_{off(i)}) + m_2 T_{off(i)} \tag{A.3}$$

Where $T_{off(i)}$ is the i_{th} cycle off-time. Assuming that the perturbed off-time

$$T_{off(i)} = T_{off} + \Delta T_{off(i)} \tag{A.4}$$

Where the T_{off} is the steady-state off-time, and $\Delta T_{off(i)}$ is the difference between the perturbed i_{th} cycle off-time $T_{off(i)}$ and the steady-state off-time T_{off}. t_i can be defined as:

$$t_i = (i-1)(T_{on} + T_{off}) + \sum_{k=1}^{i-1} \Delta T_{off(k)} \tag{A.5}$$

Now $\Delta T_{off(i)}$ can be found from equation 3.3 as it is shown in below equation:

$$m_2 \Delta T_{off(i)} = v_c(t_{i-1} + T_{off(i-1)}) - v_c(t_i + T_{off(i)}) \tag{A.6}$$

Therefore, $\Delta T_{off(i)}$ becomes:

$$\begin{aligned}
\Delta T_{off(i)} &= \frac{1}{m_2}\widehat{r}\{sin[2\pi f_m \cdot (t_{i-1} + T_{off(i-1)}) - \theta] - sin[2\pi f_m \cdot (t_i + T_{off(i)}) - \theta]\} \\
&\approx -\frac{1}{m_2}\widehat{r} \cdot 2cos[\pi f_m \cdot (t_{i-1} + t_i + 2T_{off}) - \theta] \cdot sin(\pi f_{mT_{sw}}) \\
&\approx -2\frac{1}{m_2}\widehat{r} \cdot sin[\pi f_m \cdot (T_{on} + T_{off})] \cdot cos[2\pi f_m(i-1)(T_{on} + T_{off}) - \frac{T_{on} - T_{off}}{2}]
\end{aligned} \tag{A.7}$$

The pertubed inductor current $i_L(t)$ can be defined as in equation A.8:

$$i_L(t)|_{0\leq t\leq t_M + T_{off(M)} + T_{on}} = \int_0^t [\frac{V_i}{L}d(t)|_{0\leq t\leq t_M + T_{off(M)} + T_{on}} - \frac{V_o}{L}]dt + i_{Lo} \tag{A.8}$$

Applying the fourier analysis on the inductor current, the resulted fourier coefficient of the inductor current $C_{m(iL)}$ at the perturbation frequency f_m is simplified below:

$$\begin{aligned}
C_{m(iL)} &= \frac{j2\pi f_m}{N\pi} \int_0^{t_M + T_{off(M)} + T_{on}} i_L(t) \cdot e^{-j2\pi f_m t} dt \\
&= -\frac{1}{N\pi}\frac{V_i}{L}e^{-j2\pi f_m T_{off}}(1 - e^{-j2\pi f_m T_{on}})[\sum_{i=1}^M (e^{-j2\pi f_m(i-1)T_{sw}} \cdot \sum_{k=1}^i \Delta T_{off(k)})]
\end{aligned} \tag{A.9}$$

From the equation 3.7 and 3.9, the following expressions are obtained:

$$
\begin{aligned}
C_{m(iL)} &= -\frac{1}{N\pi}\frac{V_i}{L}e^{-j2\pi f_m T_{off}}\left(1-e^{-j2\pi f_m T_{on}}\right)\cdot\left\{-2\frac{\widehat{r}}{m_2}sin[\pi f_m\cdot T_{sw}]\right\}\cdot\sum_{i=1}^{M}\{e^{-j2\pi f_m(i-1)T_{sw}}\cdot \\
&\quad \sum_{k=1}^{i}cos[2\pi f_m[(k-1)T_{sw}-\frac{T_{on}-T_{off}}{2}]-\theta]\} \\
&= -\frac{1}{N\pi}\frac{V_i}{L}e^{-j2\pi f_m T_{off}}\left(1-e^{-j2\pi f_m T_{on}}\right)\cdot\left\{-2\frac{\widehat{r}}{m_2}sin[\pi f_m\cdot T_{sw}]\right\}\cdot\frac{1}{2}\sum_{i=1}^{M}\{e^{-j2\pi f_m(i-1)T_{sw}}\cdot \\
&\quad \sum_{k=1}^{i}\{e^{j[2\pi f_m[(k-1)T_{sw}-\frac{T_{on}-T_{off}}{2}]-\theta]}+e^{-j[2\pi f_m[(k-1)T_{sw}-\frac{T_{on}-T_{off}}{2}]-\theta]}\}\} \\
&= \frac{1}{N\pi}\frac{V_i}{L}e^{-j2\pi f_m T_{off}}\left(1-e^{-j2\pi f_m T_{on}}\right)\cdot\left\{2\frac{\widehat{r}}{m_2}sin[\pi f_m\cdot T_{sw}]\right\}\cdot\frac{1}{2}\sum_{i=1}^{M}\{e^{-j2\pi f_m(i-1)T_{sw}}\cdot \\
&\quad \sum_{k=1}^{i}\{e^{j[2\pi f_m[(k-1)T_{sw}-\frac{T_{on}-T_{off}}{2}]-\theta]}+\sum_{k=1}^{i}e^{-j[2\pi f_m[(k-1)T_{sw}-\frac{T_{on}-T_{off}}{2}]-\theta]}\}\}
\end{aligned}
\tag{A.10}
$$

$$
\begin{aligned}
&\sum_{i=1}^{M}\{e^{-j2\pi f_m(i-1)T_{sw}}\cdot\{\sum_{k=1}^{i}e^{j[2\pi f_m[(k-1)T_{sw}-\frac{T_{on}-T_{off}}{2}]-\theta]}\}\} \\
&= e^{-j\theta}\cdot e^{-j2\pi f_m\frac{T_{on}-T_{off}}{2}}\cdot\sum_{i=1}^{M}\{e^{-j2\pi f_m(i-1)T_{sw}}\cdot[\sum_{k=1}^{i}e^{j2\pi f_m(k-1)T_{sw}}]\} \\
&= e^{-j\theta}\cdot e^{-j2\pi f_m\frac{T_{on}-T_{off}}{2}}\cdot\sum_{i=1}^{M}\{e^{-j2\pi f_m(i-1)T_{sw}}\cdot\frac{1-e^{j2\pi f_m iT_{sw}}}{1-e^{j2\pi f_m T_{sw}}}\} \\
&= e^{-j\theta}\cdot\frac{e^{-j2\pi f_m\frac{T_{on}-T_{off}}{2}}}{1-e^{j2\pi f_m T_{sw}}}\sum_{i=1}^{M}\{e^{-j2\pi f_{m(i-1)}T_{sw}}-e^{j2\pi f_m T_{sw}}\} \\
&= e^{-j\theta}\cdot\frac{e^{-j2\pi f_m\frac{T_{on}-T_{off}}{2}}}{1-e^{-j2\pi f_m T_{sw}}}\cdot M
\end{aligned}
\tag{A.11}
$$

$$
\begin{aligned}
&\sum_{i=1}^{M}\{e^{-j2\pi f_m(i-1)T_{sw}}\cdot\{\sum_{k=1}^{i}e^{-j[2\pi f_m[(k-1)T_{sw}-\frac{T_{on}-T_{off}}{2}]-\theta]}\}\} \\
&= e^{j\theta}\cdot e^{j2\pi f_m\frac{T_{on}-T_{off}}{2}}\cdot\sum_{i=1}^{M}\{e^{-j2\pi f_m(i-1)T_{sw}}\cdot[\sum_{k=1}^{i}e^{-j2\pi f_m(k-1)T_{sw}}]\} \\
&= e^{j\theta}\cdot e^{j2\pi f_m\frac{T_{on}-T_{off}}{2}}\sum_{i=1}^{M}[e^{-j2\pi f_m(i-1)T_{sw}}\cdot\frac{1-e^{-j2\pi f_m iT_{sw}}}{1-e^{-j2\pi f_m T_{sw}}}] \\
&= e^{j\theta}\cdot\frac{e^{j2\pi f_m\frac{T_{on}-T_{off}}{2}}}{1-e^{-j2\pi f_m T_{sw}}}\sum_{i=1}^{M}[e^{-j2\pi f_m(i-1)T_{sw}}\cdot(1-e^{-j2\pi f_m iT_{sw}})] \\
&= e^{j\theta}\cdot\frac{e^{j2\pi f_m\frac{T_{on}-T_{off}}{2}}}{1-e^{-j2\pi f_m T_{sw}}}\sum_{i=1}^{M}(e^{-j2\pi f_m(i-1)T_{sw}}-e^{-j2\pi f_m(2i-1)T_{sw}})=0
\end{aligned}
\tag{A.12}
$$

Now, it can be found that:

$$
\begin{aligned}
C_{m,L} &= \frac{1}{2}\frac{1}{N\pi}\frac{V_i}{L}e^{-j2\pi f_m T_{off}}\left(1-e^{-j2\pi f_m T_{on}}\right)\cdot\left\{2\frac{\widehat{r}}{m_2}sin(\pi f_m\cdot T_{sw})\right\}\cdot e^{-j\theta}\cdot\frac{e^{-j2\pi f_m\frac{T_{on}-T_{off}}{2}}}{1-e^{-j2\pi f_m T_{sw}}}\cdot M \\
&= \frac{V_i}{L\cdot j2\pi f_m}\frac{j2\pi f_m M}{N\pi}\frac{\widehat{r}}{m_2}sin(\pi f_m T_{sw})\cdot e^{-j\theta}\cdot\frac{e^{-j2\pi f_m\frac{T_{sw}}{2}}\left(1-e^{-j2\pi f_m T_{on}}\right)}{1-e^{-j2\pi f_m T_{sw}}} \\
&= \frac{V_i}{L\cdot j2\pi f_m}j2f_s\frac{\widehat{r}}{m_2}sin(\pi f_m T_{sw})\cdot e^{-j\theta}\cdot\frac{\left(1-e^{-j2\pi f_m T_{on}}\right)}{e^{j\pi f_m T_{sw}}-e^{-j\pi f_m T_{sw}}} \\
&= \frac{V_i}{L\cdot j2\pi f_m}j2f_s\frac{\widehat{r}}{m_2}sin(\pi f_m T_{sw})\cdot e^{-j\theta}\cdot\frac{\left(e^{-j2\pi f_m T_{on}}-1\right)}{2jsin(\pi f_m T_{sw})} \\
&= \frac{V_i}{L\cdot j2\pi f_m}\widehat{r}\frac{f_s}{m_2}\left(1-e^{-j2\pi f_m T_{on}}\right)e^{-j\theta}
\end{aligned}
\tag{A.13}
$$

Finally, the transfer function from the control to the inductor current can be found as:

$$
\frac{i_L(s)}{v_c(s)} = \frac{C_{m,L}}{\widehat{r}\cdot e^{-j\theta}} = \frac{f_s}{m_2}\left(1-e^{-sT_{on}}\right)\frac{V_i}{Ls}
\tag{A.14}
$$

The exponential term $e^{-sT_{on}}$ can be simplified as shown in equation A.15 using the pade' approximation.

$$
e^{-sT_{on}} = 1 - \frac{sT_{on}}{1+\frac{s}{Q_1\omega_1}+\frac{s^2}{\omega_1^2}}
\tag{A.15}
$$

where $\omega_1 = \frac{\pi}{T_{on}}$ and $Q_1 = \frac{2}{\pi}$.

By inserting the equation $e^{-sT_{on}}$ from A.15 into A.14, the expression A.16 is obtained.

$$
\frac{i_L(s)}{v_c(s)} \approx \frac{1}{R_i}\cdot\frac{1}{1+\frac{s}{Q_1\omega_1}+\frac{s^2}{\omega_1^2}}
\tag{A.16}
$$

Using the circuit diagram in Figure A.1, the inductor current can also be expressed as function of output voltage through the equations A.17.

$$
\begin{aligned}
i_L(s) &= \frac{V_o(s)}{R_{co}+\frac{1}{sC_o}}+\frac{V_o(s)}{R_L} \\
&= \frac{V_o(s)R_L+V_o(s)(R_{co}+\frac{1}{sC_o})}{(R_{co}+\frac{1}{sC_o})R_L} \\
&= V_o(s)\frac{(1+sR_{co}C_o)R_L}{(R_L+R_{co})sC_o+1}
\end{aligned}
\tag{A.17}
$$

Finally, the control to outout transfer function can be obtained in equation A.18.

$$
\frac{v_o(s)}{v_c(s)} \approx \frac{1}{R_i}\cdot\frac{1}{1+\frac{s}{Q_1\omega_1}+\frac{s^2}{\omega_1^2}}\cdot\frac{R_L(R_{co}C_os+1)}{(R_L+R_{co})C_os+1}
\tag{A.18}
$$

The LTC3810 B

LTC3810 is the current mode sychronous switching regulator which is able to operate witht input voltage up to 100V. LTC3810 has 28 pins as it can be seen in Figure B.1.
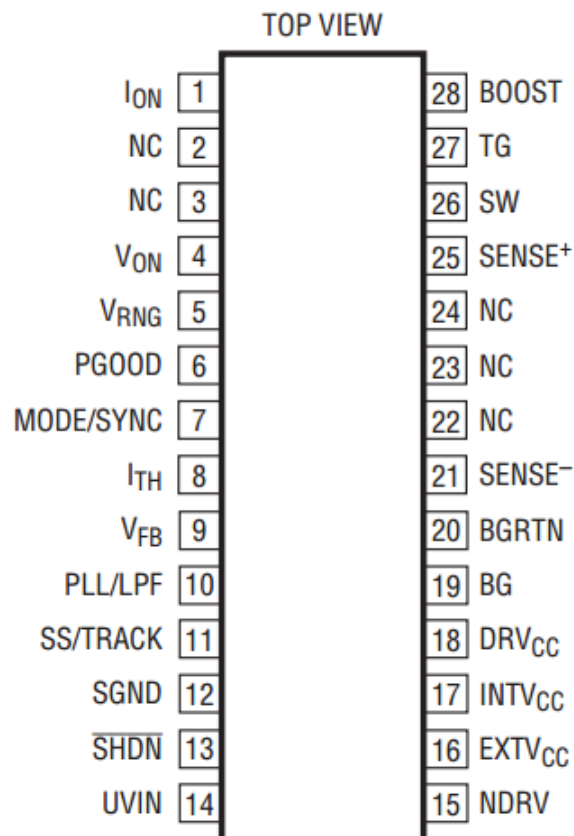
TOP VIEW

I_{ON}	1		28	BOOST
NC	2		27	TG
NC	3		26	SW
V_{ON}	4		25	SENSE⁺
V_{RNG}	5		24	NC
PGOOD	6		23	NC
MODE/SYNC	7		22	NC
I_{TH}	8		21	SENSE⁻
V_{FB}	9		20	BGRTN
PLL/LPF	10		19	BG
SS/TRACK	11		18	DRV_{CC}
SGND	12		17	$INTV_{CC}$
$\overline{SHDN}$	13		16	$EXTV_{CC}$
UVIN	14		15	NDRV

Figure B.1. The LTC3810 pin configuration; [technology [2007]]

Some of these pin's functions are described below:

- Pin1, I_{ON} : This pin is the on-time current input. The resistor can be connected between pin1 and the input voltatge to set the switching frequency
- pin4, V_{ON}: On time voltage input. This pin makes the the on-time proportional to the output voltage.
- Pin5, V_{RNG}: Sense voltage limit set. The pin5 is connected to the resistive divider from $INTV_{cc}$, and this sets the nominal sense voltage at maximum output current.
- Pin7 $MODE/SYNC$: Pulse Skip Mode Enable/Sync pin. This pin provides pulse skip mode enable/disbale control and an external clock input to the phase detector.
- Pin8, I_{TH}: Error Amplifier compensation point and current control threshold.
- Pin9, V_{FB}: Feedback input. This pin is connected to the output voltage through a resistor divider network.

- Pin10, PLL/LPF: This pin is connected to the phase-locked loop's lowpass filter.
- pin11, $SS/TRACK$: Soft-Start/Tracking Input. The low capacitor is tied from this pin to ground in order to set the ramp rate of the output voltage.
- Pin12, $SGND$: Signal ground. All small signals are connected to this ground.
- Pin13, $SHDN$: Shutdown Pin. The voltage under 1.5V will turn off both of the external MSFET Q_1 and Q_2, thereby shutdown the LTC3810.
- Pin14, $UVIN$: Uvlo Input. This pin is connected to the input voltage through the resistive divider, and the voltage on this pin is compared to 0.8V reference. When UVIN is under 0.8V, the LTC3810 is shut down.
- Pin15, $NDRV$: Drive Output for External Pass Device of the linear regulatot for $INTV_{CC}$. This is connected to the gate of the external NMOS pass device and a pull up resistor to the input voltage V_{in}.
- Pin16, $EXTV_{cc}$: External driver supply voltage. When the volage is above 6.7V, this pin will be connceted to $INTV_{cc}$, and will turn off the external MOSFET connceted to $NDRV$.
- Pin17, $INTV_{CC}$: Main supply Pin. This pin supply the power to all internal circuits.
- Pin18, DRV: Driver supply. DRV supplies power to the BG output driver.
- Pin19, BG: Bottom Gate Drive. The BG pin drives the gate of the bottom N-channel synchronous switch MOSFET.
- Pin20, $BGRTN$: Bottom gate return. It connects the source of the pull-down MOSFET in BG driver.
- Pin21 and 25: Current sense comparator input. Sense(+) is connected to SW and sense(-) is used to sende the bottom side of the on-resistor mosfet.
- Pin26, SW: Switch Node Connection to inductor and Bootstrap capacitor
- Pin27, TG: Top gate driver. The TG pin drives the gate of the top N-channel sychronous switch Mosfet.
- Pin28, $Boost$: Top Gate Driver supply. This pin supplies power to the top gate driver.

PCB design C

The Figure C.1 shows PCB schematic with 2 layers (Top and bottom) that was designed using Eagle Software. The red lines represent the wires on the top layer, and the blue lines represent the wires on the bottom layers.
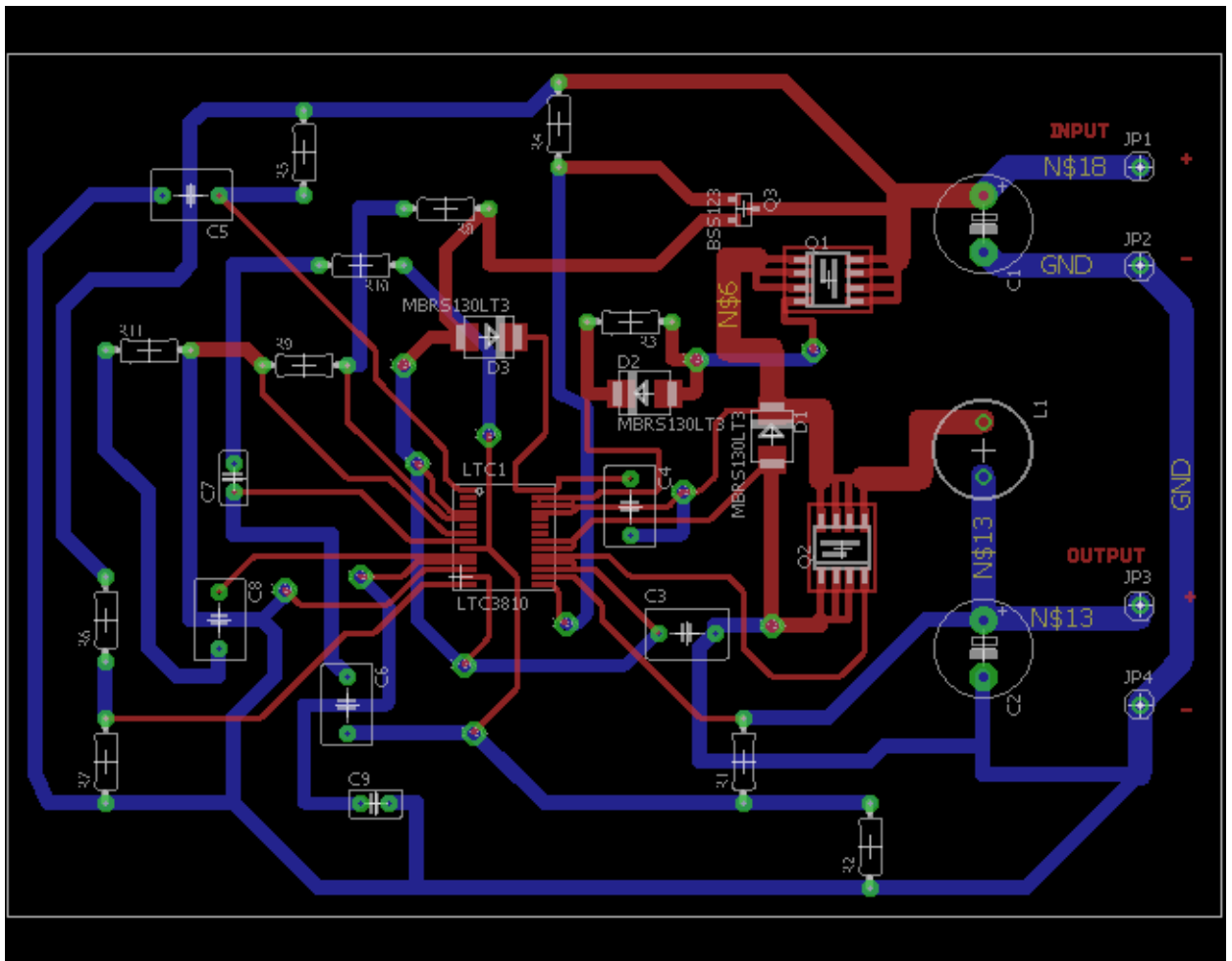

Figure C.1. The PCB board schematic

After designing the 2 layers PCB, some components were mounted as shown in Figure C.4. Some of the designed components were not available at the moment. In this case, they were replaced by those which have kind of similar properties. In the beginning of test, the PWM signal could not show up at the gate of the Top MOSFET (Q_1), and this may be due to the used components which are different from designed ones. The other reason could also be the short circuit which occured somewhere on board. It was not possible to complete the test in that moment because there were short time left since I started to build the converter; because most of the time was spent on analysing and designing the converter and the controller.
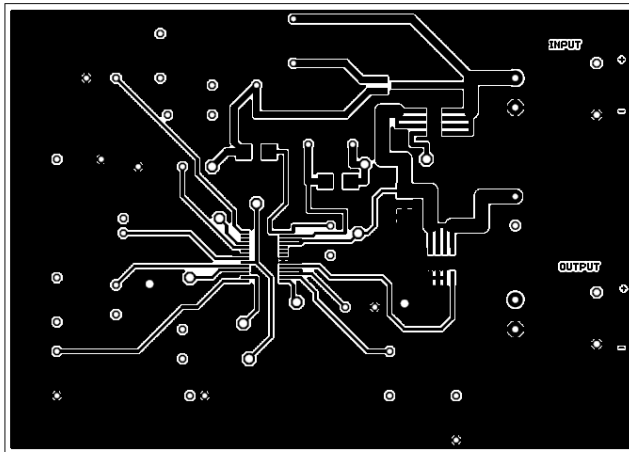
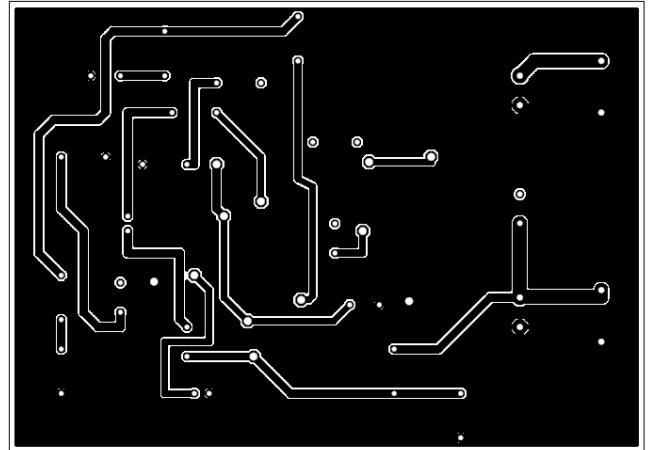**Figure C.2.** The PCB board on Top layer
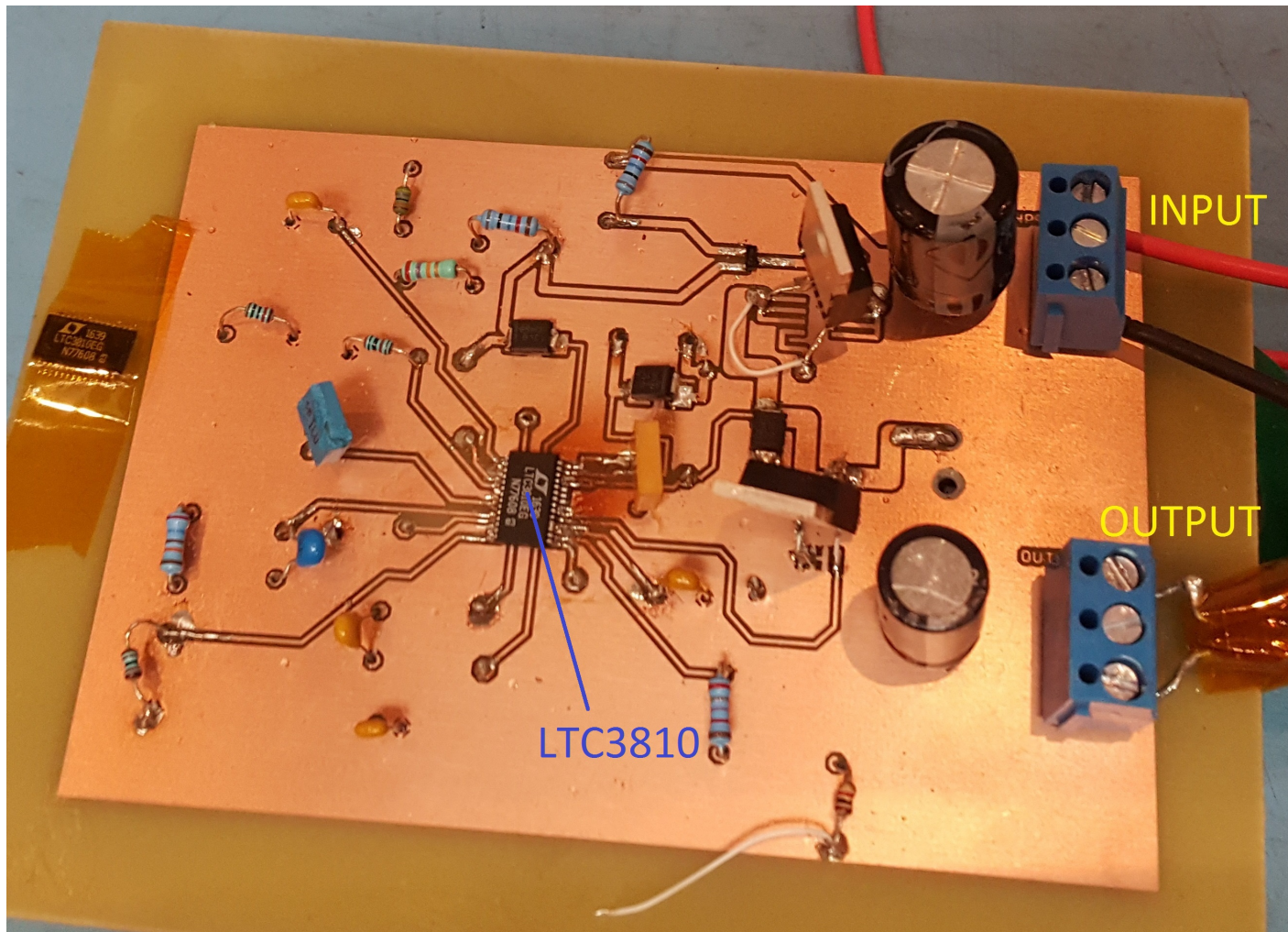

Figure C.3. The PCB board on bottom layer

INPUT

OUTPUT

LTC3810

Figure C.4. The printed PCB setup